2010

Damage detection in composite interfaces through carbon nanotube reinforcement

Bily, Mollie A.

Monterey, California. Naval Postgraduate School

NPS-MAE-10-003

NAVAL POSTGRADUATE SCHOOL

MONTEREY, CALIFORNIA

DAMAGE DETECTION IN COMPOSITE INTERFACES THROUGH CARBON NANOTUBE REINFORCEMENT

by

Mollie A. Bily, Young W. Kwon, and Randall D. Pollak

12 February 2010

Approved for public release; distribution is unlimited.

Prepared for: Air Force Office of Scientific Research (AFOSR), Arlington VA.

THIS PAGE INTENTIONALLY LEFT BLANK

NAVAL POSTGRADUATE SCHOOL
Monterey, California 93943-5000

Daniel T. Oliver
President

Leonard A. Ferrari
Executive Vice President and Provost

This report was prepared for and funded by the Air Force Office of Scientific Research (AFOSR).

This report was prepared by:

_____
Mollie A. Bily
Lieutenant, United States Navy

_____
Young W. Kwon
Professor
Department of Mechanical and
Astronautical Engineering

_____
Randall D. Pollak
Lt Col, United States Air Force
Department of Mechanical and
Astronautical Engineering

Reviewed by:

_____
Knox T. Millsaps
Chairman
Department of Mechanical and
Astronautical Engineering

Released by:

_____
Karl van Bibber
Vice President and Dean of Research

THIS PAGE INTENTIONALLY LEFT BLANK

REPORT DOCUMENTATION PAGE

Form Approved
OMB No. 0704-0188

1. REPORT DATE	**2. REPORT TYPE**	**3. DATES COVERED** *(From - To)*
10, February 2010	Technical Report	April 2009 - February 2010

4. TITLE AND SUBTITLE
Damage Detection in Composite Interfaces through Carbon Nanotube Reinforcement

5a. CONTRACT NUMBER
F1ATA09134G002 (MIPR)

5b. GRANT NUMBER

5c. PROGRAM ELEMENT NUMBER

6. AUTHOR(S)
Mollie A. Bily, Young W. Kwon and Randall D. Pollak

5d. PROJECT NUMBER

5e. TASK NUMBER

5f. WORK UNIT NUMBER

7. PERFORMING ORGANIZATION NAME(S) AND ADDRESS(ES)
Naval Postgraduate School
Monterey, CA 93943

8. PERFORMING ORGANIZATION REPORT NUMBER
NPS-MAE-10-003

9. SPONSORING / MONITORING AGENCY NAME(S) AND ADDRESS(ES)
Air Force Office of Scientific Office (AFOSR)
Arlington, VA

10. SPONSOR/MONITOR'S ACRONYM(S)

11. SPONSOR/MONITOR'S REPORT NUMBER(S)

12. DISTRIBUTION / AVAILABILITY STATEMENT
Approved for public release; distribution is unlimited

13. SUPPLEMENTARY NOTES The views expressed in this report are those of the author and do not reflect the official policy or position of the Department of Defense or the U.S. Government.

14. ABSTRACT
Use of carbon nanotubes along composite interfaces was studied to both improve fracture strength and monitor interfacial damage progression. Both carbon fiber and E-glass fiber composites were manufactured with vinyl ester resin using vacuum-assisted resin transfer molding. First, the effects of single-step curing (i.e., co-curing) versus two-step curing (i.e., curing a new section to a previously cured section) was studied using Mode II fracture testing. The results showed the two-step cured interface was as strong as the co-cured interface, thus validating the use of two-step curing during modular construction or repair of composite sections. Application of carbon nanotubes to the composite interfaces was then accomplished through two-step curing, using acetone as a dispersant. Mode II testing indicated significant improvement of the interface fracture toughness for both carbon fiber and glass fiber samples with carbon nanotubes. Because carbon nanotubes have very high electrical conductivity, the electrical resistance was measured across the interface during Mode II loading. As the interface crack grew, there was an increase in electrical resistance (approximately linear for carbon fiber specimens until final failure). The study demonstrated the feasibility of electrical resistance measurement with dispersed carbon nanotubes to monitor damage along critical interfaces, while simultaneously improving fracture properties.

15. SUBJECT TERMS Carbon Nanotubes, Structural Health Monitoring, Crack Growth, Crack Propagation, Resistance Testing

16. SECURITY CLASSIFICATION OF:			**17. LIMITATION OF ABSTRACT**	**18. NUMBER OF PAGES**	**19a. NAME OF RESPONSIBLE PERSON**
a. REPORT Unclassified	**b. ABSTRACT** UU	**c. THIS PAGE** U	Unclassified	86	**19b. TELEPHONE NUMBER** *(include area code)*

Standard Form 298 (Rev. 8-98)
Prescribed by ANSI Std. Z39.18

THIS PAGE INTENTIONALLY LEFT BLANK

TABLE OF CONTENTS

LIST OF FIGURES

I. INTRODUCTION

A. MOTIVATION

In the past decade, composite structures have been in the forefront of structural research. For example, the Department of the Navy has looked at both carbon fiber and fiberglass composites for use in construction of ship superstructures, submarine sails, and structures of unmanned aircraft.[1] Many promising steps have been taken to ensure that composites are increasingly integrated into structural use. However, a recurring hindrance to successful integration of composite structures is the ability to withstand failure in critical areas of stress concentration, especially in those areas where discontinuities in the reinforcing material (e.g., fibers) are present, such as the joints between composite sections or at composite/metal interfaces. Often, the failures in such regions are matrix-dominated – i.e., the weaker matrix material of the composite fails due to interply delamination, bonding failure between the matrix and adhesive (in the case of adhesive joints), or other failure mode not avoidable through the use of high-strength reinforcing material such as continuous fibers.[2]

Perhaps even more important than the ability to withstand failure is the ability to detect damage and thereby predict failure before it occurs. Thus, the design challenge for large composite structures is not only designing for strength in high-stress structural weak points, but also designing for confidence in safety and reliability at those weak points by ensuring structural integrity. Such confidence is a result of in situ monitoring or periodic inspections which can detect and monitor defects (cracks, delaminations, etc.) before they progress to a critical stage. As composite materials are generally non-homogeneous with unique failure modes, detecting such damage can be more difficult than with traditional engineering metals, especially at joints and other areas where: (a) geometries are more complex, (b) there may be adhesives, fasteners, dissimilar structural materials, and/or

[1] A.P. Mouritz, E. Gellert, P. Burchill, and K. Challis, "Review of Advanced Composite Structures for Naval Ships and Submarines," *Composite Structures* 53 (2001): 21–41.

[2] R. Jones, H. Alesi, W.K. Chiu, and S. Galea, "A Preliminary Study into the Matrix Dominated Non-linear Behavior of Graphite/Epoxy Laminates," *Composite Structures* 30 (1995): 193-199.

other material non-linearities, and (c) in situ sensing equipment can decrease strength due to additional stress concentration effects.

The Navy's F/A-18 program had to deal with the challenge of incorporating large composite structures while ensuring structural integrity in a demanding operational environment. The F/A-18 helped pioneer the use of composite-to-metal interfaces as a primary load path through the design of the composite wing.[3] The composite wing is bonded to the titanium root using a step lap joint between the graphite epoxy and titanium. During developmental testing, delamination was discovered in the joint and subsequent detailed testing showed matrix-dominated delamination within the composite to be the dominant failure mechanism at the joint (rather than failure of the adhesive used to bond the wing to the root). According to Boeing engineers, bolts were added to the step lap joint to provide confidence in the structural integrity, although testing may not have necessarily justified their need or effect.[4] However, the presence of traditional fasteners in the design provided managers added confidence in the structural integrity of the joint. It could be argued that this confidence was misplaced, as the addition of the fasteners may have actually reduced the joint's strength, but they may have enhanced the ability to detect critical damage before catastrophic failure.

Similar materials issues have been faced in the commercial development of the Boeing 787 Dreamliner and the civil development of NASA's Ares/Constellation launch system. Both systems have incorporated large composite structures to a much greater degree than used in the past for such applications, and both have required much effort to address concerns regarding the reliability and durability of such structures. One of the recent challenges faced by the 787 team has also been in the area of the wing root.[5] The wings are stiffened by composite stringers attached to the skin and titanium root, and flexural stresses encountered in testing led to delamination issues at the highly-loaded wing roots, requiring redesign of the stringers and addition of fastener bolts along the top of the wing, causing significant delays to the development schedule. The Ares program

[3] R. Jones and H. Alesi. "On the Analysis of Composite Structures with Material and Geometric Non-linearities," *Composite Structures* 50 (2000): 417-431.

[4] R. Grounder (The Boeing Company). Personal communications, 8 Aug 2008.

[5] D. Gates. "Boeing 787 May not Fly this Year," *The Seattle Times*, 22 Jul 2009.

had evaluated composites for many of the structural components.[6] Despite performance advantages of composite materials, some of these components are now incorporating more traditional alloys due to manufacturing concerns and to enhance confidence in structural integrity, such as the design of the J-2X extended rocket nozzle. The J-2X is to be the largest nozzle extension shell ever used on a liquid-propelled rocket and was planned to be made of a carbon fiber composite, but was changed to an aluminum-based design in later iterations despite the potential lower performance and higher weight.[7]

These examples illustrate the need for improved mechanisms to simultaneously strengthen and provide health monitoring of critical interfaces in order to fully realize the potential of large composite structures for military, civil, and commercial applications.

B. CARBON NANOTUBES

Carbon nanotubes (CNTs) have received much attention for a wide variety of applications since their discovery almost two decades ago, and remain at the forefront of nanotechnology research to solve the most vexing engineering problems. Carbon-carbon bonds are amongst the strongest of chemical bonds found in nature, and are the basis for the strength of carbon nanotubes. CNTs are made of sp^2 hybridized carbon bonds, with each atom joined to three neighbors creating a hexagonal lattice structure like that found in sheets of graphite (i.e., graphene).[8] The lattice structure forms a tube with a nano-sized diameter and can be several millimeters in length, as shown in Figure 1.

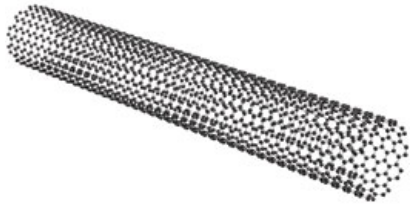

Figure 1. Single-walled carbon nanotube.[9]

[6] R. Messinger. "Evaluation of Advanced Composite Structures Technologies for Application to NASA's Vision for Space Exploration," NASA Technical Report, NASA/CR-2008-215120, Jul 2008.

[7] Government Accountability Office (GAO). "NASA: Constellation Program Cost and Schedule Will Remain Uncertain Until a Sound Business Case Is Established," GAO Report 09-844, 25 Sep 2009.

[8] R. Saito and M. S. Dresselhaus, *Physical Properties of Carbon Nanotubes* (Imperial College Press, 1998), 11–12.

[9] The Venton Research Group. Development of Carbon Nanotube Modified Microelectrodes. n.d. http://www.faculty.virginia.edu/ventongroup/nanotube.html (accessed September 9, 2009).

CNTs may be classified as single-walled, double-walled, or multi-walled, based on the number of concentric graphene sheets making up the nanotube. Although many strides have been made in the manufacturing of CNTs, they are still quite expensive (on the order of $100s per gram). CNTs have an extremely high elastic modulus (greater than 1 TPa), high tensile strengths (up to 63 GPa), and are extremely lightweight, making them ideal for reinforcement of composite materials.[10] One concern in the use of carbon nanotubes is their propensity to cluster due to attraction between the nanotubes. Figure 2 shows scanning electron microscope (SEM) images of a cluster of multi-walled CNTs (from the Materials Laboratory of the Naval Postgraduate School's Department of Mechanical and Astronautical Engineering).

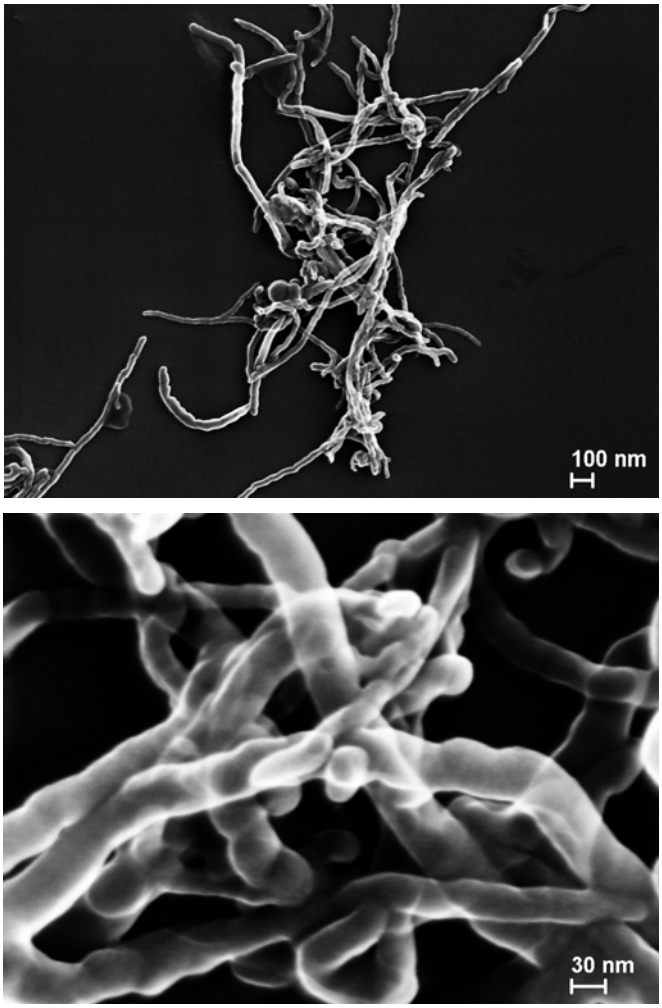

Figure 2. SEM images of clustered CNT network.

[10] P.J.F. Harris. "Carbon Nanotube Composites," *International Materials Review* 49 (2004): 31.

It has already been demonstrated that inclusion of CNTs in areas of high stress concentration can increase a material's ability to withstand stress at these critical areas.[11] However, a secondary benefit could be the use of CNTs to monitor composite materials to detect damage in such areas. Compared to metals, the failure of composites can be much more insidious due to the accumulation of damage within the heterogeneous structure of dissimilar materials with a variety of different failure modes, ultimately leading to component failure.[12] The health monitoring potential of CNTs arises from their very high electrical conductivity (in general). When properly dispersed within a less conductive media, a network of CNTs can increase the electrical conductivity. As damage progresses within the component, this network is disrupted and the electrical conductivity should decrease, which can be measured as an increase in electrical resistance. Thus, employing a network of CNTs at a critical juncture would provide a dual purpose for their inclusion in the composite material. Composite materials could be strengthened at key points, while simultaneously detecting interfacial damage. By reinforcing only at key points (rather than dispersing throughout the composite matrix), the costs of adding CNTs are not overly prohibitive for large structures.

C. LITERATURE REVIEW

Recent studies have been conducted which advance the feasibility of damage detection in composite materials through the use of CNTs. During one study, a CNT-enhanced polymer material was used to fabricate a piezoresistive strain sensor for structural health monitoring. This sensor proved to have a linear symmetric strain response under static and dynamic loading, however the CNTs were only included within the sensor itself.[13] A similar study showed that multidirectional strains could be measured using an isotropic film of CNTs placed on a four-point probe. This probe then

---

[11] Susan Faulkner, *Study of Composite Joint Strength with Carbon Nanotube Reinforcement,* Naval Postgraduate School, MS thesis, September 2008, 1–42.

[12] I. Weber, and P. Schwartz, "Monitoring Bending Fatigue In Carbon-Fibre/Epoxy Composite Strands: A Comparison Between Mechanical and Resistance Techniques," *Composites Science and Technology* 61 (2001): 849–853.

[13] I. Kang, M.J. Schulz, J.H. Kim, V. Shanov, and D. Shi, "A Carbon Nanotube Strain Sensor for Structural Health Monitoring," *Smart Materials and Structures,* 15 (2006): 737–748.

could be moved around to different locations sensing a linear strain response in all locations.[14]

Another study focused solely on the use of CNTs as a replacement for strain gauges.[15] This study placed semi-conductive multiwall CNT-fiberglass–epoxy polymer composites under both tensile and cyclic loading to detect failure. It was shown that the multiwall CNTs were able to outperform regular strain gauges in sensing different types of failures. This was due to their ability to be interspersed within the composite and, as a result, be more sensitive to the changing stress fields around them. The use of such embedded strain gauges could provide valuable information on the actual loads experienced in service by composite components.

In addition to work done on strain gauges, very recent research has been conducted using CNTs to monitor crack progression. In one study, CNTs were first dispersed into a polymer matrix and then infiltrated into layers and bundles of conventional fibers. Thostenson and Chou used this percolated network as a sensor to detect the onset, nature, and evolution of damage in an advanced polymer-based composite.[16] A similar study demonstrated that a network of CNTs throughout the composite material is an effective way to monitor fatigue-induced damage, as well as provide opportunities for damage repair.[17] A follow-on study by Thostenson and Chou showed that a high aspect ratio was necessary throughout the entire network of CNTs to ensure high conductivity to allow for damage detection.[18] They also investigated CNTs as a means to monitor the structural integrity of a mechanically-fastened composite

---

[14] P. Dharap, Z. Li, S. Nagarajaiah, and Barrera, E.V, "Nanotube Film Based on Single-Wall Carbon Nanotubes for Strain Sensing," *Nanotechnology,* 15 (2004): 379–382.

[15] M. Nofar, S.V. Hoa, and M.D. Pugh, "Failure Detection and Monitoring in Polymer Matrix Composites Subjected to Static and Dynamic Loads Using Carbon Nanotube Networks," *Composites Science and Technology* (2009): 1–22.

[16] E.T. Thostenson and T. Chou, "Carbon Nanotube Networks: Sensing of Distributed Strain and Damage for Life Prediction and Self Healing," *Advanced Materials,* 18 (2006): 2837–2841.

[17] W. Zhang, V. Sakalkar, and N. Koratkar, "In Situ Health Monitoring and Repair In Composites Using Carbon Nanotube Additives," *Applied Physiscs Letters,* 91 (2007).

[18] T. Chou and E.T. Thostenson. "Carbon Nanotube/Vinyl Ester Nanocomposites for in Situ Sensing," September 17-29, 2008. University of Maryland University College, Adelphia, MD. *Office of Naval Research Solid Mechanics Program Review Meeting: Marine Composites and Sandwich Structures:* 42–49.

joint.[19] Additional studies have also given insight into the use of electrical conductivity as a means to quantify disruption of CNT networks, thereby enabling detection and monitoring of material damage.[20, 21, 22] In general, in just the last three years, exploitation of the electrical conductivity of CNT networks for use in composite structures has drawn increasing interest by a number of researchers.

Previous investigations of CNTs for health monitoring generally used a network of CNTs dispersed throughout the composite base material to enable damage detection. Although they indicated the potential for such detection, such an approach may not address interfacial damage mechanisms. In order to achieve this type of damage detection, a layer of CNTs percolated along the matrix surface needs to be studied. Such a localized approach has economic benefits as well, as the very expensive CNTs are used only in critical areas such as joints and stress concentrations, rather than dispersed throughout the composite material. This localization may be especially beneficial for large composite structures which are fabricated or repaired by joining modular sections.

D. OBJECTIVES

The objective of this research is to advance the uses of CNTs within composite materials to detect and monitor damage at critical interfaces, while simultaneously enhancing the fracture properties at such interfaces.

Previous research showed that CNTs can increase the fracture toughness of the composite interface significantly; however, only one assembly mode (two-step cured) was studied.[23] The first objective of this research is to determine the critical strain energy release rate, G, and crack propagation characteristics of a carbon fiber vinyl ester resin composite during Mode II fractures for both single-step cured (i.e., co-curing two

---

[19] E.T. Thostenson and T. Chou. "Carbon Nanotube-based Health Monitoring of Mechanically Fastened Composite Joints," *Composites Science and Technology*, 68 (2008): 2557-2561.

[20] F. Deng and Q. Zheng. "An Analytical Model of Effective Electrical Conductivity of Carbon Nanotube Composites," Applied Physics Letters, 92 (2008).

[21] C. Lu and Y. Mai. "Anomalous Electrical Conductivity and Percolation in Carbon Nanotube Composites," *Journal of Materials Science*, 43 (2008): 6012-6015.

[22] K. Ahmed, W. Pan, and S. Shi. "Electrical Conductivity and Dielectric Properties of Multiwalled Carbon Nanotube and Alumina Composites," *Applied Physics Letters*, 89 (2006).

[23] Faulkner, "Study of Composite Joint Strength with Carbon Nanotube Reinforcement," 15–42.

sections along the interface) and two-step cured (i.e., curing one section to a previously cured section) composite sample sets. This comparison will help determine whether two-step curing of carbon fiber composites degrades mechanical properties compared to co-curing. If the results are similar, the methods could be interchanged and allow for more flexibility in the composite material assembly process. More significantly for this study, it would be desirable for two-step curing to not degrade the integrity of the interface, as two-step curing makes the application of a CNT layer along the interface much more practical. Thus, this initial research phase serves as a prerequisite to the use of a dispersed CNT layer along an interface using two-step curing.

If it can be shown that two-step curing does not significantly diminish fracture properties, the next step is to validate previous recent research suggesting that the addition of CNTs of a given type and specified concentration (based on capability to enhance fracture toughness) does indeed enhance fracture properties of carbon fiber and glass fiber composites during Mode II loading. By independently fabricating a new set of samples through the vacuum-assisted resin transfer molding (VARTM) process, confidence in previous test results can be ensured.

If it can be validated that the addition of a CNT layer during such two-step curing will enhance fracture properties, the final phase of this research is to exploit the electrical conductivity of CNT networks in order to monitor damage along the composite interface. Such damage (namely, crack growth along the interface) should disrupt the CNT network, thus affecting the electrical conductivity as measured by an increase in electrical resistance. When damage has progressed to the point that CNTs are no longer touching each other, the electrical resistance should be a maximum. A procedure using electrical current to test for damage would provide a relatively simple method for maintenance inspections or in situ health monitoring. The added advantage of such an approach is that the sensors (i.e., the CNT network) are simultaneously improving the fracture properties. This double benefit (less susceptibility to damage while providing means to detect damage) can make composite materials more attractive for those military, civil, and commercial applications where confidence in safety and reliability are paramount.

II. COMPOSITE SAMPLE CONSTRUCTION

A. SAMPLE SPECIFICATION

Three different sample sets were constructed during this research. The first set consisted of two types of carbon fiber composite coupons: one set of coupons being co-cured, and the other set being two-step cured. The second and third sample groups also consisted of two coupon types per sample set. One coupon group was fiber composite with resin only (i.e., without a CNT layer), while the other fiber composite group was CNT-reinforced. The differences between the second and third sample sets were the type of base reinforcing material used, being carbon fiber and fiberglass, respectively.

Each sample set consisted of the same basic coupon construction, with varying parameters, and materials. All coupons had pre-existing cracks built into them in order to represent an area of high-stress concentration. The basic parameters are depicted in Figure 3, while the second and third sample sets also had stainless steel metal sheets built into each end to allow for current to run through the sample sets. For these two sample sets of coupons, the length of the crack was made sufficiently longer so that the extra width of the thin piece of metal did not affect the test results.

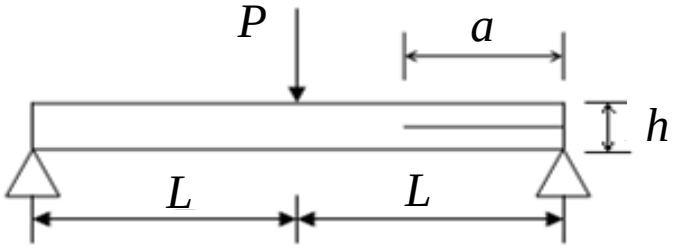

Figure 3. Geometry of samples under load.

where: 2L = length
h = thickness
a = initial crack length
P = applied load

B. MATERIALS

Sample sets one and two were both constructed of TORAY T700CF carbon fiber weave with a vinyl-ester matrix whose base was DERAKANE 510–A. The third sample set also used DERAKANE 510–A to create the base, but this time was made with bidirectional fiberglass woven roving. Typically, fiberglass woven roving is categorized by weight in ounces per square yard; for this research, 24-oz per square-yard E-glass woven roving was used. Both the carbon fiber weave and the fiberglass woven were chosen based on their current use in DoD structural projects.

In order to make the vinyl ester matrix, the DERAKANE 510–A had to be cured and hardened. The hardening chemicals used for this process are methyl ethyl ketone peroxide (MEKP) and cobalt naphthenate (CoNap). MEKP was used to initiate the chemical reaction to cure the DERAKANE 510–A, while CoNap was used to ensure that the reaction occurred in the desired cure time. For this research, the desired cure time was 60 minutes, which provided enough time for the DERAKANE to completely penetrate all layers of the woven materials.

The above two hardeners work well if the ambient temperature is between 70˚F and 80˚F, in which case the combination of hardeners was 1.25 weight percent MEKP and 0.20 weight percent CoNap. For most of the research, the ambient temperature was below 70˚F and a third chemical, N-dimthylaniline (DMA), was needed to ensure a cure time of 60 minutes. When DMA was used in combination with the previously stated weight percentages for CoNap and MEKP, a total of 0.05 weight percent of DMA was required. If DMA was not included at these lower room temperatures, cure times would be much longer than the desired 60 minutes.

C. VACUUM-ASSISTED RESIN TRANSFER MOLDING

One technique for making composite materials in industry is vacuum-assisted resin transfer molding (VARTM), which was used in this project to construct the three different sample sets required for testing. The VARTM process uses a vacuum to pull resin through the many layers of fiber to ensure a uniform distribution of resin throughout

the sample. This technique was extremely beneficial when working with CNTs, as they did not shift or move when the resin was run through the sample.

To begin making the two-step cured samples, a layer of peel ply was placed on a piece of glass to allow for easy removal of the sample upon completion of the VARTM process. The glass used must be at least 1.27 cm (0.5 in) thick, in order to be able to withstand the extreme heat generated during the resin curing process. When making a co-cured sample, a layer of distribution media is laid down first, covered by a layer of peel ply, as shown in Figures 4 and 5.

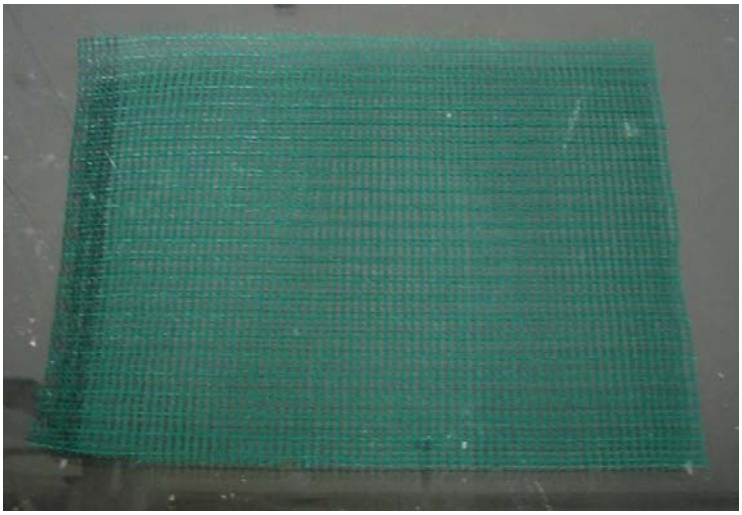

Figure 4. Bottom layer of distribution media used for co-cured samples.

Figure 5. Peel ply laid on top of distribution media for co-cured samples.

Next, the sample size was chosen and the fiber materials were cut to the appropriate size. For all samples, 10 layers of fabric were cut, five for the bottom layer, and five for the top layer. The bottom five layers were then placed on top of the peel ply, as shown in Figure 6. For the co-cure process, a Teflon® film of thickness 0.0051 cm (0.002 in) was placed partially on top of the bottom five layers in order to build a crack into the sample. The last five layers of fiber material were evenly stacked on top of the fiber material and Teflon® already in place. Then another layer of peel ply, followed by a piece of distribution media, was stacked on top of the complete co-cure sample. For the double-cure sample, the bottom five layers were covered with the peel ply and distribution media, as shown in Figure 7.

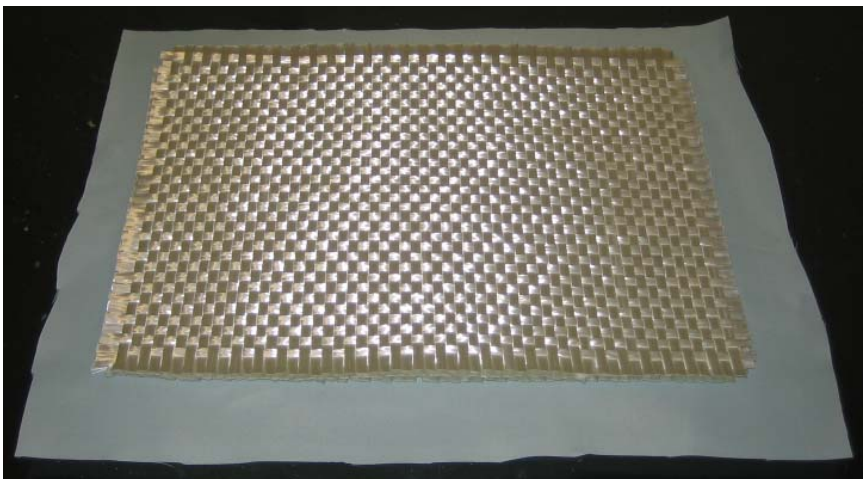

Figure 6. Bottom five layers of a sample.

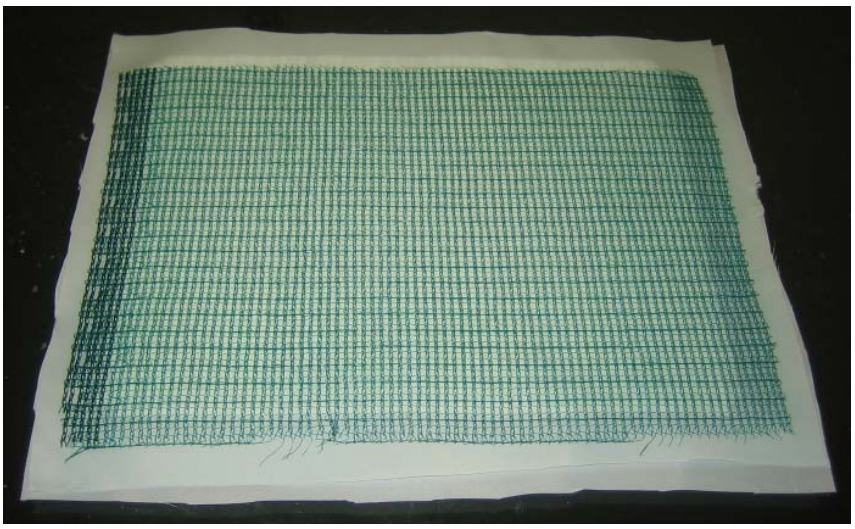

Figure 7. Peel ply and distribution media on top of stacked fiber layers.

In order for the resin to be pulled through the fiber material, a Rietschel Thomas Vacuum Pump model 2688CE44 was used. Tubing was hooked up to this pump and run through a gauge board to a resin trap, as shown in Figure 8. The resin trap was used to protect both the pump and gauge board from excess resin. From the resin trap, solid ½-inch diameter plastic tubing was measured and cut to be used inside the vacuum bag as the outlet for the resin. This same tubing was used to suck resin from the bottom of the sample to the top. Attached to both the inlet and outlet tubes, and spread across the top and bottom of the sample, was spiral tubing, as shown in Figure 9. This tubing allowed for an even distribution of the resin throughout the sample.

Figure 8. Gage board and resin trap.

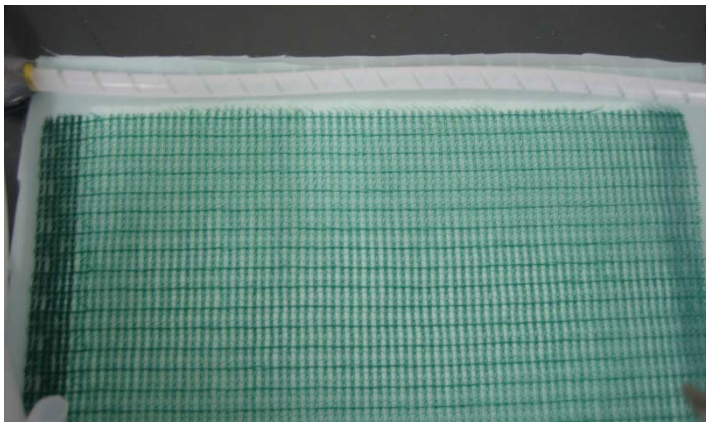

Figure 9. Spiral tubing used at the top and bottom of sample set-up.

Once the tubing was assembled and secured, strips of vacuum bag tape were laid out in a box shape around the sample stack. The strips were placed about 2 to 3 inches from the sample stack, so as not to interfere with the resin being run through the sample. The tape was used to hold the plastic sheet in place, which ultimately acted as a vacuum bag, as shown in Figures 10 and 11. The plastic sheet was cut to fit the square box already made, and was carefully rolled out onto the tape, as shown in Figures 11 and 12. The vacuum was turned on, and the newly-created bag was thoroughly checked to make sure there were no leaks. If there were to have been a leak in the bag, air bubbles would have entered both the bag and the sample, making the sample unusable. Once it had been verified there were no leaks, the vacuum was left on to ensure a continuous vacuum pressure throughout the rest of the VARTM process.

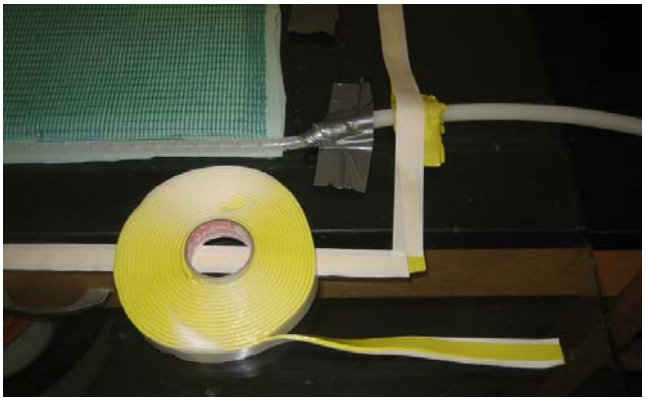

Figure 10. Vacuum tape used to seal the sample setup.

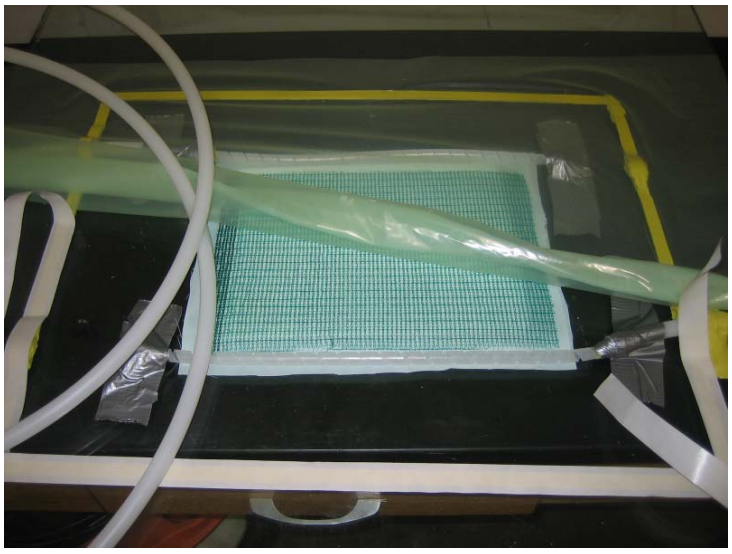

Figure 11. Rolling out the plastic sheet used to form the vacuum bag.

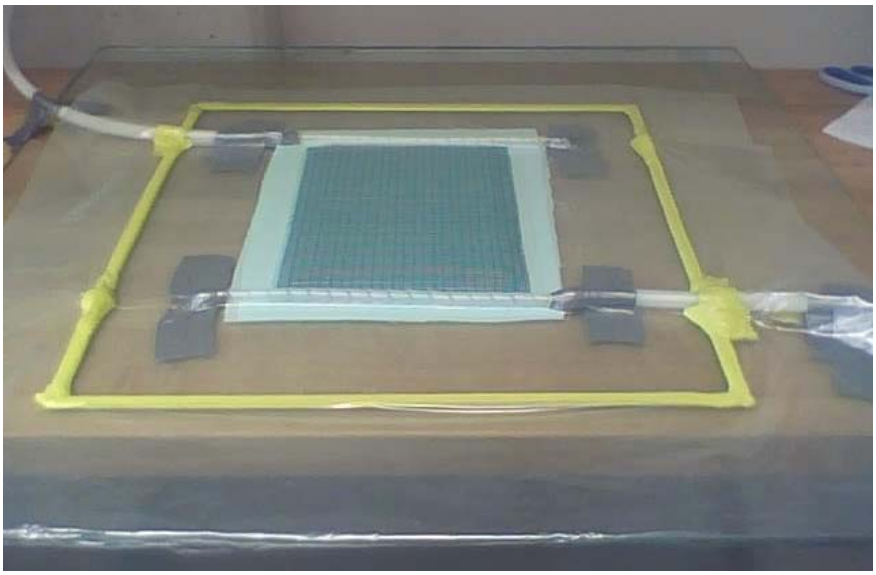

Figure 12. Sample setup under vacuum.

While the vacuum was still running, the temperature was noted and the appropriate amounts of resin and hardeners were mixed to ensure a 60-minute cure time. Once mixed, the resin was transferred to the inlet of the vacuum bag and the inlet tube was clamped to prevent the resin from flowing through the sample. As a result of mixing and transferring the resin to a new bucket, small bubbles are formed throughout the resin, seen in Figure 13. Enough time (about 10-15 minutes), was allowed for these bubbles to dissipate before running the resin through the sample. If allowed to run through the sample, these bubbles would have gotten caught and ruined the sample.

Figure 13. Resin at inlet with bubbles after mixing.

After sufficient time had passed and no small bubbles could be seen in the resin, the inlet tube was unclamped slowly to allow the resin to enter the vacuum bag. The resin flowed evenly through the sample at a steady pace, as shown in Figure 14. The resin was allowed to run all the way through the spiral tubing on the top, in order to ensure all fibers were coated with the resin as in Figure 15. One aid used to ensure that all fibers were covered with resin was the placement of the distribution media at the beginning of the VARTM setup. When both a top and bottom layer were used, the bottom distribution media hung out the bottom of the sample by about ½ inch. The top distribution media was then place under the top spiral tubing and even with the bottom of the sample. This placement aided in sucking the resin up from the bottom of the sample, through the middle, and out the top.

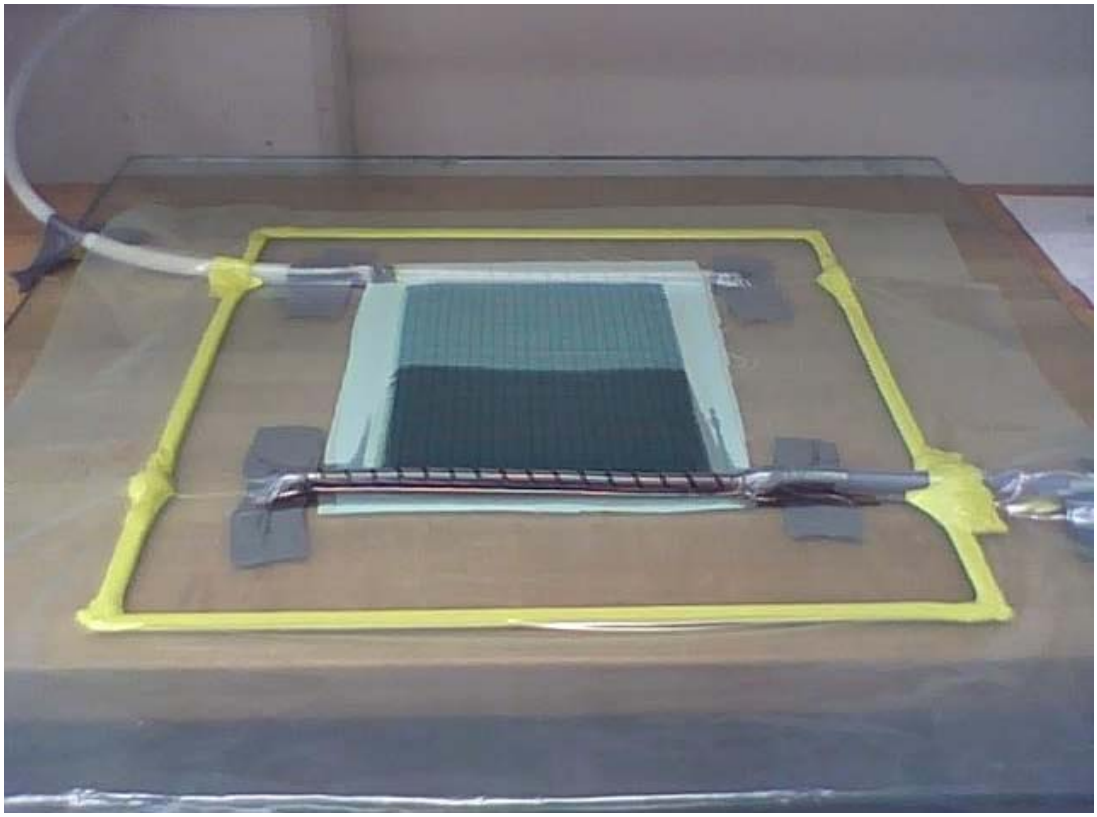

Figure 14. Resin running through a sample evenly.

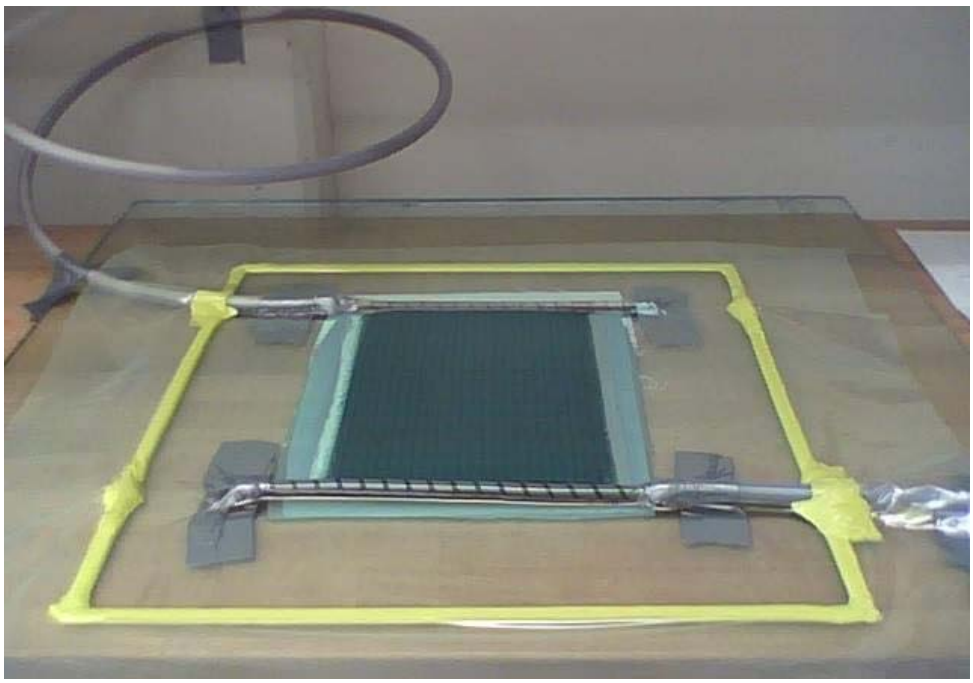

Figure 15. Resin completely through a sample.

As the resin started to cure, it became extremely hot and started to gel. When this occurred, and all the layers were covered with resin, the resin inlet tubing was again clamped to ensure no air was pulled into the sample. The time it took for this to happen depended on the thickness and size of the sample, as well as the amount of resin and hardeners used. The sample was left with the vacuum pump running until the sample cured. If the resin and hardeners were mixed and added correctly, this was about 60 minutes. After this time, the pump was shut off, but the sample was left at least 12 hours to ensure complete curing of the sample. At this point, the co-cured sample was complete and was taken to a water jet to get cut into the correct coupon size. For the two-step cured process more work was needed to complete the sample.

Since the bottom layer of the two-step cured sample was the only thing made the first time through, the initial crack and top layer were then manufactured. To do this, the first start step was to take the newly-made bottom layer, and sand the top surface with 100 grit sand paper in order to roughen the surface. Next, the sanded surface was cleaned with acetone, in order to make sure that all sanded particles are removed. The acetone was allowed to fully dry before continuing the VARTM process. When working with

CNTs, they were dispersed over the top of the entire sanded composite plate using acetone, again ensuring enough time was allowed for the acetone to dry, as shown in Figure 16.

Figure 16. Bottom layer of two-step cured sample covered with CNTs.

For sample sets two and three, thin pieces of stainless steel plates were fastened to the top and bottom of the sample, as shown above in Figure 16. The stainless steel was needed to allow for a point to secure conductive test equipment to the sample and not interfere with any other testing. For all other samples, this step was skipped.

Finally, the same steps as before were followed. Peel ply was laid on the glass followed by the bottom composite plate. The crack was formed using the same Teflon® material as before and as shown in Figure 17. The previously-cut five pieces of fiber material used to make the top plate were carefully stacked on top, shown in Figure 18. More peel ply was used, again followed by a piece of distribution media on top. Tubing was cut, tape was laid out, and the vacuum bag was sealed and tested. The resin was then mixed, allowed to sit while bubbles were popped, and then the resin was run through the sample. The resin got hot, gelled, and 60 minutes later it was completely cured and the

pump was shut off. Again, the sample was given about 12 hours to sit and fully set. Once the two-step cured plate was complete, it was taken to be cut using a water jet.

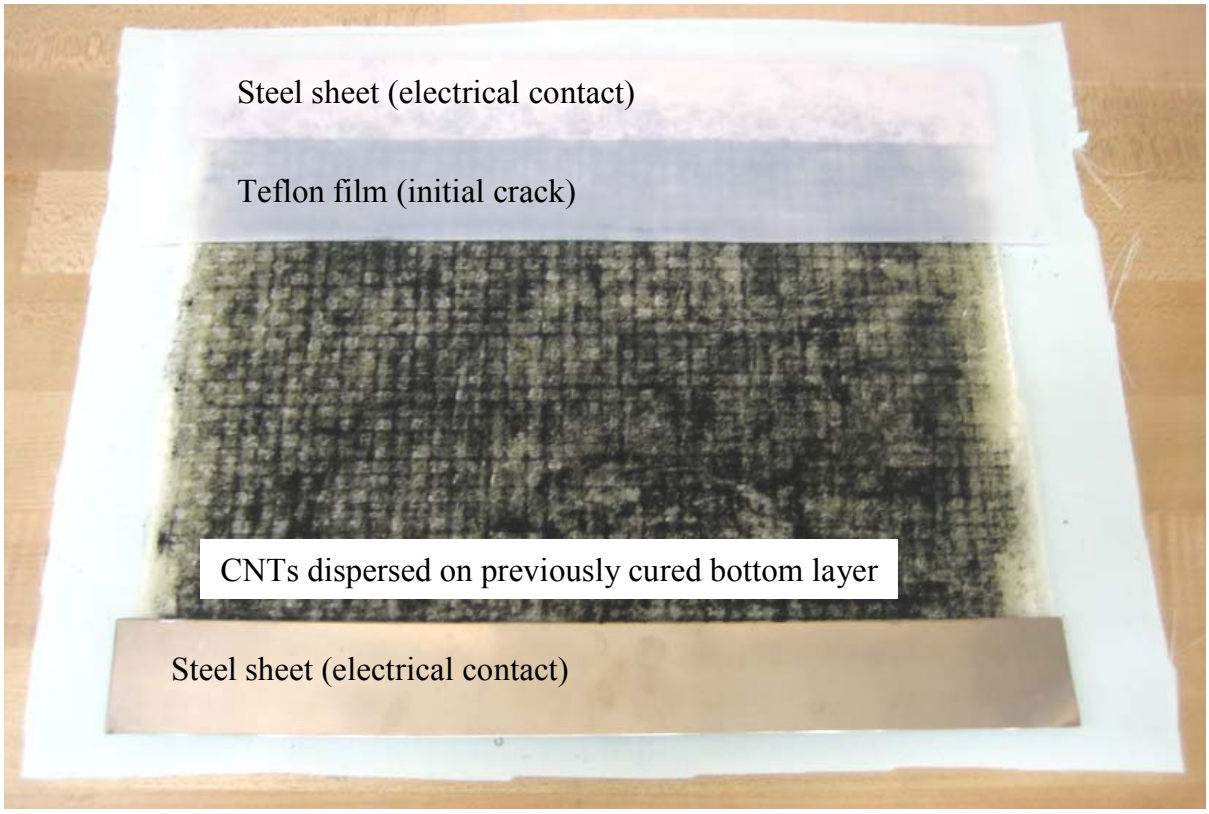

Figure 17. Teflon® layer used to build initial crack in sample.

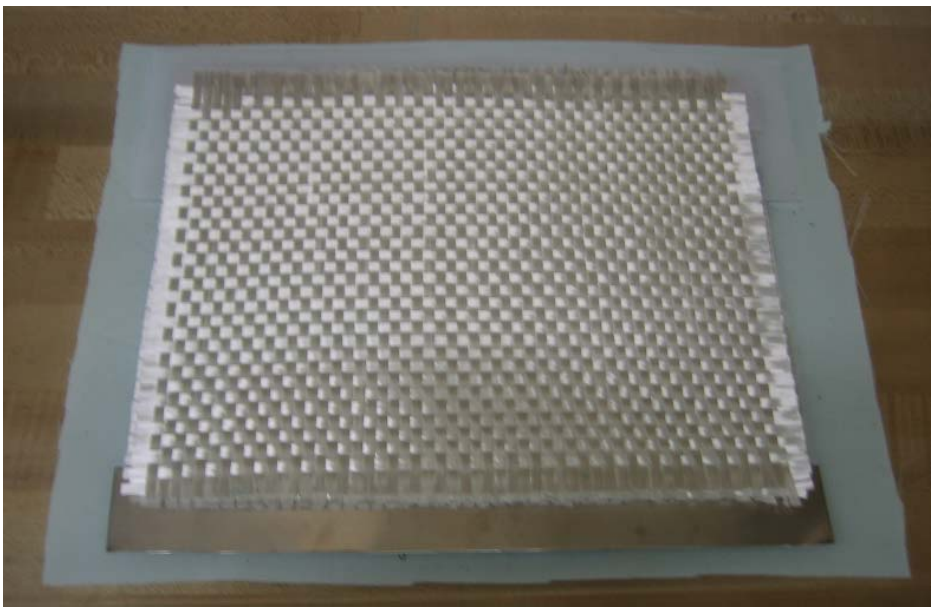

Figure 18. Remaining fiber material stacked on top of bottom plate.

THIS PAGE INTENTIONALLY LEFT BLANK

III. PHASES OF RESEARCH

A. FAMILIARIZATION (PHASE I)

Phase I consisted of a familiarization stage, during which samples were constructed by the student to learn the finer ins and outs of the VARTM technique. Many samples were constructed, but only the final few were used for this research project. During this phase, samples were fabricated and investigated to improve the fabrication process. A number of samples were cut into coupons and tested in order to increase familiarity with the test equipment, but no data were collected during this phase.

B. CO-CURED VS. TWO-STEP CURED (PHASE II)

Phase II was conducted in order to compare the results using a co-cure method versus a two-step cure method when making samples. This phase consisted of two different sets of carbon fiber composite samples that did not include CNTs. Samples were cut into coupons 2.4 cm wide, 0.42 cm thick, and 17 cm long, based on applicable ASTM standards. The coupons were tested in Mode II under three-point bending and critical strain energy release rate, G, was calculated. Comparison of G_{II} values between co-cured versus two-step cured samples was then accomplished.

C. CARBON FIBER COMPOSITE RESISTANCE TESTING (PHASE III)

Once Phase II was complete, two new carbon fiber composite sample sets were constructed. One set of samples was the same as the Phase II two-step cured samples, while the other sample set included a layer of CNTs dispersed through the center of the sample along the interface between the top and bottom layers. The CNT surface concentration was 7.5 g/m^2 and they were dispersed using acetone. The selection of CNT surface concentration, as well as the selection of acetone as the dispersing agent, was based on results from compression testing of CNT-reinforced scarf joints during previous research conducted at the Naval Postgraduate School.[24]

[24] Y.W. Kwon, R. Slaff, S. Bartlett, and T. Greene, "Enhancement of Composite Scarf Joint Interface Strength through Carbon Nanotube Reinforcement," *Journal of Materials Science* (2008): 1–9.

Additionally, built into each sample set at the ends were thin pieces of stainless steel metal, which served as contact points for electrical conductivity testing. These sample sets were then cut into the same size coupons as used in Phase II.

The purpose of this phase of research was to determine if a layer of CNTs could be used to detect crack propagation making use of the high electrical conductivity of CNTs. Both sets of samples were tested in Mode II, while an electrical current was run through them and the resistance was monitored. The resistance changes before, during, and after Mode II testing were noted for those coupons with CNT layer. The critical strain energy release rate, G, was calculated and compared for the coupons with and without CNT reinforcement.

D. FIBERGLASS COMPOSITE RESISTANCE TESTING (PHASE IV)

Upon completion of Phase III, similar-sized sample sets as used in Phase III were constructed and cut into coupons, except fiberglass was used as the base reinforcing material rather than carbon fibers. As glass fibers are orders of magnitude less conductive than carbon fibers, a higher CNT dispersion concentration of 10 g/m^2 was used to provide adequate networking to ensure electrical conductivity through the interface. The purpose of testing with fiberglass was to determine if the electrical conductivity of CNTs could be exploited in composite materials with a significantly less conductive nature. Ideally, even in low conductive materials, some current will flow through the CNT layer, allowing for crack propagation to be detected. Both sets of samples were tested in Mode II, while an electrical current was run through them and the resistance was monitored. The resistance changes before, during, and after Mode II testing were noted for the coupons with CNT layer. Critical strain energy release rate, G, was calculated and compared for those coupons with and without CNT reinforcement.

E. RESISTANCE RELIABILITY AND CRACK GROWTH RELATIONSHIP TESTING (PHASE V)

This phase put both the carbon fiber and fiberglass composites reinforced with CNTs in Phases III and IV through more testing. This testing was designed to determine the reliability of the resistance readings collected in Phases III and IV, as well as

determine if there is a relationship between the changes in crack length and the changes in resistance. Thus the two key questions to be addressed were:

(1) Are the measured increases in resistance actually due to crack growth?

(2) Is there a relationship between crack length and electrical resistance?

To address the first question, it was necessary to measure the electrical resistance of samples before loading, and then load so that no crack growth would occur, and then remeasure the resistance. If one is to use the conductivity of the CNT layer as a damage monitoring sensor, it is important that significant increases in electrical resistance do not occur during general loading with no additional crack growth. If the CNT layer's conductivity is significantly affected by load cycles in which no macroscopic damage accumulates, this health monitoring approach may have limited practical value.

The first testing in this phase used the previously cracked sample sets with CNTs from both Phases III and IV, and slowly loaded them to a desired load prior to the point of further crack propagation. The resistance readings were then read while under load, and then upon unloading of the sample. This step was then repeated several times to determine the consistency of the resistance readings.

To address the second question in this research phase, the crack length acquired during previous testing of each coupon was measured along with the corresponding resistance reading. The cracked coupon was then placed under a high enough load for the crack to propagate. Upon propagation of the crack, and while still under load, a resistance reading was taken. The load was removed and another resistance reading was measured. This procedure was repeated until it was no longer possible to propagate the crack further. The resulting data was used to determine relationships between change in crack length and change in resistance readings.

THIS PAGE INTENTIONALLY LEFT BLANK

IV. TESTING

A. EQUIPMENT

All tests were conducted using an Instron Tension/Compression Machine (Model Number: 4507/4500), shown in Figure 19. All testing phases were conducted using a 10-kN load cell. Collection of data generated by the Instron was done by a Series IX computer software which was also used to control the Instron to achieve desired test requirements. Additionally, for Phase III, IV, and V, the coupons were hooked up to a Fluke 8840A multi-meter as displayed in Figure 20. This device was used to measure the resistance within the coupons throughout the entire test period. Data produced from this machine was collected by hand at 30-second intervals.

Figure 19. Mode II test setup in Instron test machine.

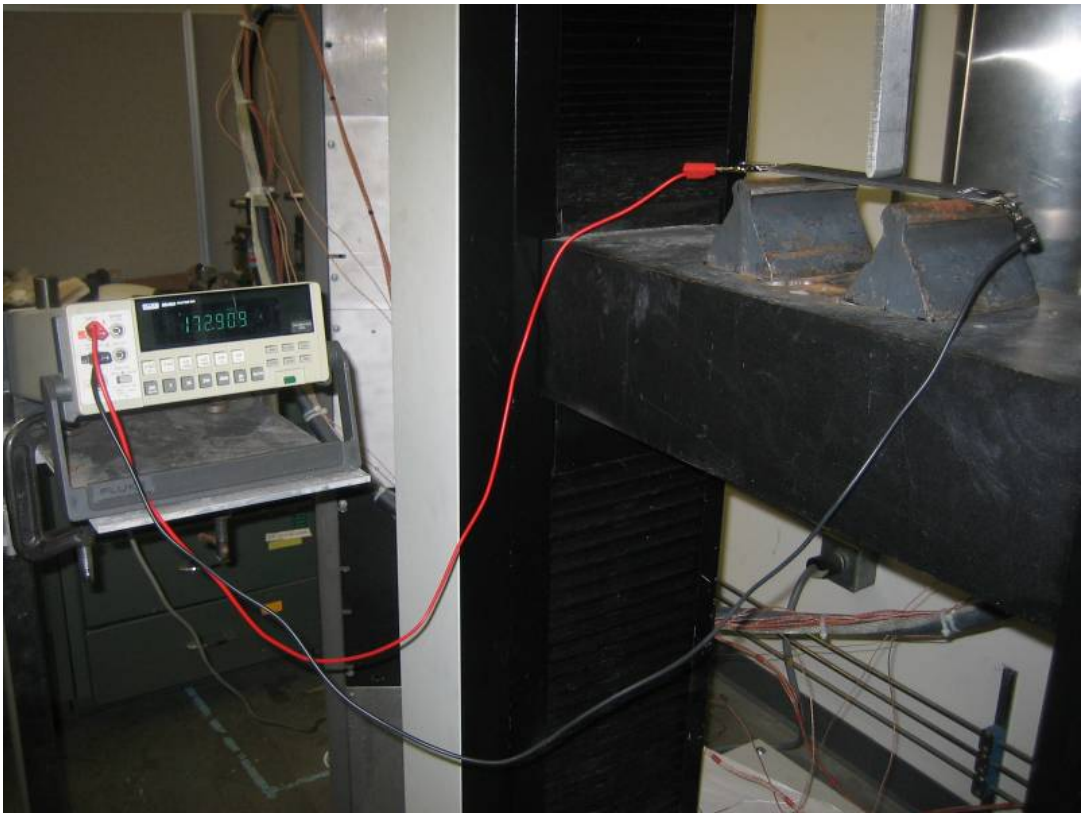

Figure 20. Fluke 8840A multi-meter and Instron Mode II test setup.

B. PROCEDURE

In order to model a Mode II fracture, in which only shear force affects crack propagation, each sample set was tested using a three-point bending test. This test was chosen based on previous research conducted.

The setup used is shown in Figures 21 and 22. For all tests, the Instron held the center support stationary, attached to the load cell, while the base supports were incrementally moved up into the stationary support. The higher the base moved the greater the load felt on the coupon became, resulting in higher shear stresses felt at the crack tip. A plot of force versus displacement was provided from the Series IX computer software and used to help calculate the Mode II critical strain energy release rate, G_{II}.

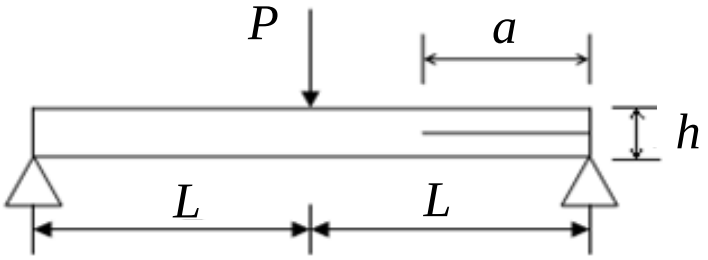

Figure 21. Schematic of three-point bending test for Mode II.

Figure 22. Picture of three-point bending test for Mode II.

Additionally, during Phase III, IV and V testing, the resistance of each coupon was monitored. At the point of crack propagation, the resistance through the coupon was annotated and compared to that of the initial resistance reading. The resistance was again taken after the test had stopped and the coupon was still bent. Another reading was taken after the coupon was removed from the Instron and returned to a load free state.

C. CALCULATIONS

In order to calculate the Mode II critical strain energy release rate, G_{II}, a compliance method was used, which is based on the slope of the load versus

displacement obtained during testing; i.e., a linear slope before crack propagation. Once the compliance is obtained, the following equation is used to calculate G_{II}:[25]

$$G_{II} = \frac{9a^2 P_c^2 C}{2b(2L^3 + 3a^3)}$$

The initial crack length (a), coupon width (b), and the span length (2L) are all dependent on coupon geometry pre-determined prior to the start of the test. The critical load, P_c, was determined based on the local maximum or slope change in the load versus displacement curve, as well as observation. Compliance was determined after the completion of the test by taking the inverse of the slope of the load versus displacement prior to crack propagation.

The compliance method is actually one of two ways to calculate G_{II}. The first method based on the Modified Beam Theory method requires material properties to be known, as well as precise measurement of height and thickness of the samples. The second method, the compliance approach, was chosen as it does not require material properties to be known. Although it could easily be determined what these material properties are, they vary depending on the CNT included and the thickness of coupon. The compliance approach indirectly measures the material properties when calculating the compliance.

No additional calculations were required for Phase III and IV resistance testing. All data collected were already in the desired form of resistance measurements. For Phase V, the slopes of the lines formed by data points on the crack length versus resistance graphs were calculated.

[25] M. Todo, T. Nakamura, and K. Takahashi, "Effects of Moisture Absorption on the Dynamic Interlaminar Fracture Toughness of Carbon/Epoxy Composites," *Journal of Composite Materials* 34 (2000): 630–648.

V. RESULTS AND DISCUSSION

A. FAMILIARIZATION (PHASE I)

During this phase, several samples were made although very few were useable. The first four sets of samples constructed were four times thicker than those ultimately tested in follow-on phases. The first two of these samples did not turn out properly due to a leak in the vacuum bag seal that, even after repair, allowed too much air in to salvage the sample. The third sample did not turn out to be good due to the thickness of the sample, and the inability of the pump to completely pull the resin through the entire sample. To fix this problem, on the fourth sample an extra strip of distribution media was used in the middle bottom portion of the sample. This allowed for three different paths for the resin to follow, ensuring the middle of the sample was thoroughly infused with resin. On most days this sample would have turned out correctly, but it never gelled in time allowing air to enter in. It was discovered that the relatively cool temperatures of Monterey CA (less than 70 degrees for most of the year in the laboratory) necessitated the addition of N-dimthylaniline (DMA) to ensure proper resin cure times.

The last two samples constructed in Phase I were used to ensure that all procedures consistently worked. With the use of DMA included in the resin and hardener mixture, all samples were made successfully. These samples were not put through Mode II testing, but were used to test new cutting techniques. Normally, samples of this nature were cut into coupons using a water jet, but after trial and error it was determined that a band saw with the correct blade would also cut composite samples quite well.

B. CO-CURED VS. TWO-STEP CURED (PHASE II)

The first coupon tested was a two-step cured coupon with a 2.6 cm initial crack length, span length of 15 cm, and width of 2.4 cm. The load was applied in the middle of the span length at a location of 4.9 cm from the crack tip. Prior to signs of crack propagation, this coupon failed at the point of the load application. This failure mode was not desired, and so the displacement rate was slowed down to 0.5 mm/min from 1 mm/min. This was meant to ensure that the bending stress within the sample would not exceed the failure stress before the crack propagated to failure.

The second coupon, tested with the new test speed, was also a two-step cured coupon with the same geometry. Again, the coupon failed at the point of load application prior to any crack propagation. Since the crack length was relatively small compared to the span length, critical bending stresses were reached prior to the onset of crack propagation. To correct for this problem, the base supports on the Instron were moved closer together, leading to a span length of 12 cm as the ideal span length for the testing in this phase. After trial and error, the ratio of crack length to one-half the span length for the test speed of 0.5 mm/min needed to be greater than 0.4 for the carbon fiber composite samples to avoid exceeding critical bending stresses prior to crack propagation.

Once a set span length was acquired, test results showed a slight increase in G_{II} for two-step cured coupons over that of co-cured coupons, although this increase was not statistically significant at the $\alpha = 0.05$ level (i.e., a two-sided 90% confidence interval). Figure 23 shows the normalized average values of G_{II}, showing the five two-step cured coupons with G_{II} values 3.8% higher on average than the six co-cured coupons. The G_{II} calculations for each coupon are tabulated in Appendix A, Section A.

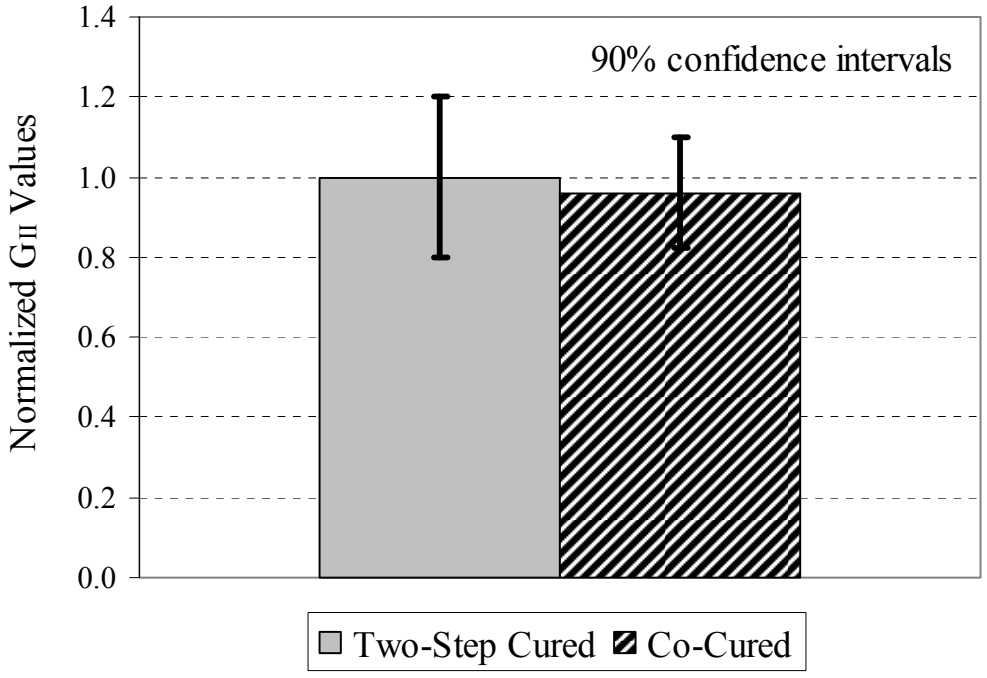

Figure 23. Normalized mean values of G_{II} for carbon fiber composite samples with two-step and one-step curing.

Upon further investigation, it was observed that the crack propagation was similar for both the two-step cured and co-cured sample sets. For both cases, the crack initially propagated from the built-in crack tip and ran along the centerline of the coupon perpendicular to the load application. Figures 24 and 25 show the path of crack propagation as described.

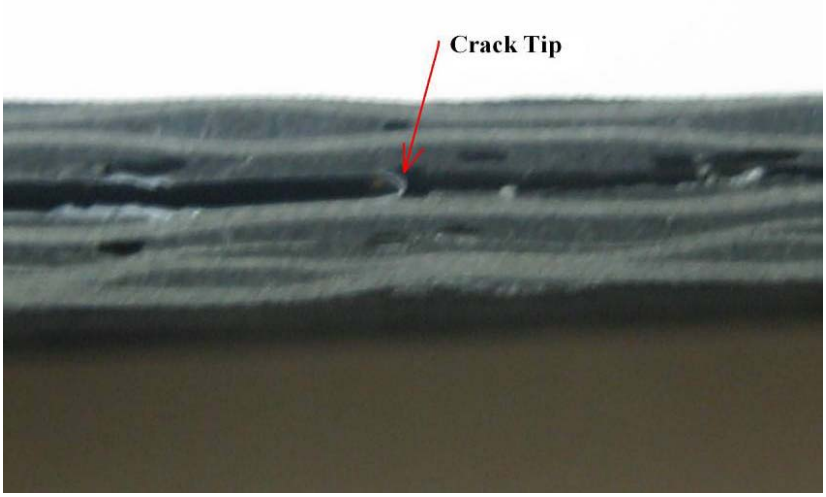

Figure 24. Crack propagation path for a co-cured carbon fiber coupon.

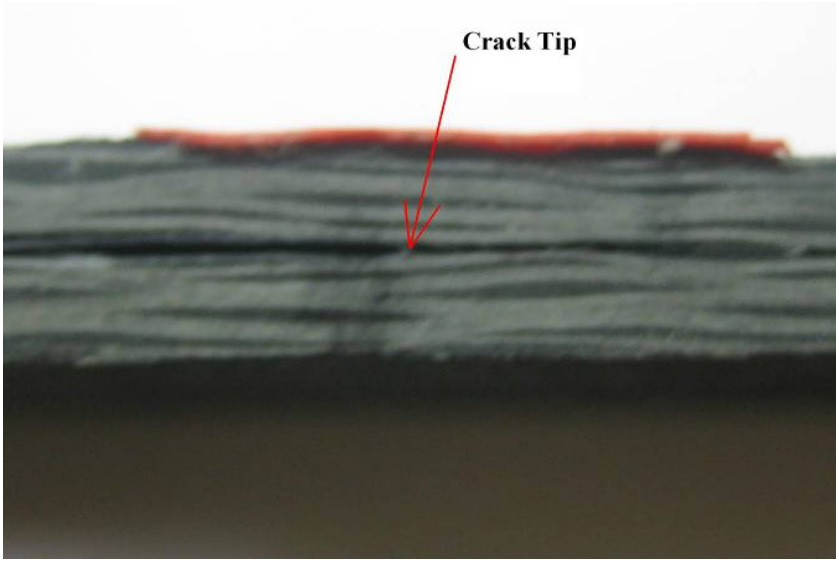

Figure 25. Crack propagation path for a two-step cured carbon fiber coupon.

After testing was complete, coupons in which crack propagation occurred were pulled apart to inspect the cracked surface. Both the co-cured and two-step cured coupons experienced the same type of failure. In some areas, the joint interface bond was

broken through the resin, while in others the resin was pulled away from the fibers, as shown in Figures 26 and 27.

Figure 26. Surface crack propagation path for a co-cured coupon.

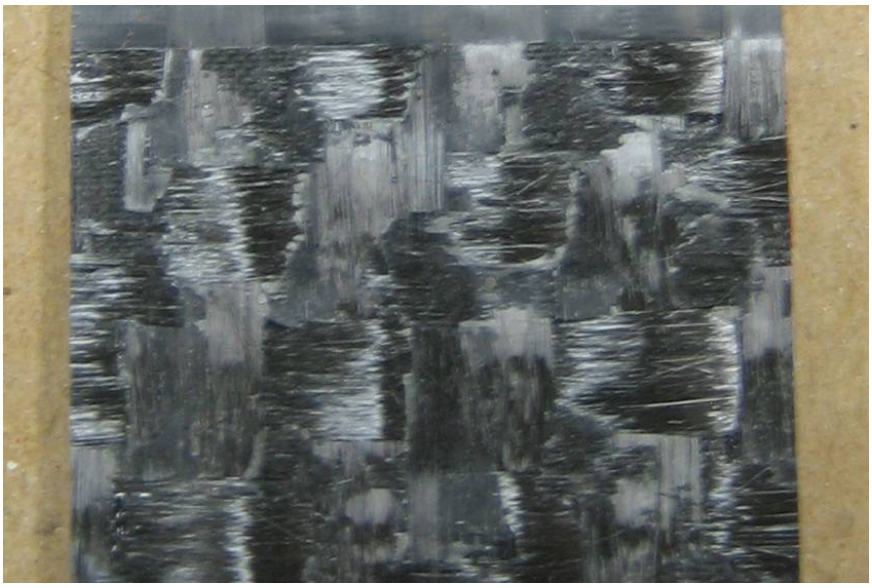

Figure 27. Surface crack propagation path for a two-step cured coupon.

Since the co-cured and two-step cured samples failed in a similar manner, a possible cause for the two-step cured higher G_{II} values is related to the VARTM process. Since the surface of the bottom resin layer is sanded and cleaned carefully with acetone when fabricating two-step samples, micro-scale defects like voids in the resin layer may

be reduced, allowing for a stronger boundary interface to form between the top and bottom layers. Again, however, the slight increase in G_{II} was not statistically significant.

C. CARBON FIBER COMPOSITE RESISTANCE TESTING (PHASE III)

This phase began with Mode II testing of all carbon fiber composite coupons containing CNTs. Based on Phase II results, a ratio of crack length to one-half the span length of greater than 0.4 was desired; as a result, the initial crack length was chosen to be 4 cm, with a span length of 16 cm, and width of 2.4 cm. These geometry parameters resulted in a ratio of 0.5, which with a Mode II test speed of 1 mm/min, resulted in coupon failure through crack propagation.

Prior to the start of testing each coupon was measured to determine its resistivity for baseline comparisons. Each of these starting resistance readings can be seen in Appendix A, Section B, which shows a varying degree of starting resistances. This variability is due to the unevenly spread CNT, directly resulting from the dispersion technique used during the VARTM process. Each value recorded, however, was constant to within a tenth of an ohm, and was read several different times before recording values. So, coupon-to-coupon variability is due to each coupon having a physically different dispersed CNT network, but each network then has a very stable electrical resistivity.

During the actual testing, values of the resistance readings were recorded manually at 30 second intervals. These values varied little from the initial readings throughout the entire test. In fact, most of the averages of these readings, with the exception of those coupons with higher initial resistance readings, matched within 14% of the initial resistance readings. Even when the sample cracked and continued to crack, the resistance readings stayed constant varying only a few ohms at a time. The average resistance readings throughout the test are also summarized in Appendix A, Section B.

When the test was complete the sample was left in the bent position shown in Figure 28. The readings taken in the bent position were again constant, only fluctuating to the tenth of an ohm, and within 4% of the initial resistance values. When the coupons were released from this bent position, the resistance readings for all coupons increased, as shown in Appendix A, Section B. Again the variance in the increase percentage can be

attributed to the CNT dispersion method used during the VARTM process. On average, the increase in resistance readings for carbon composite coupons with a layer of CNTs was 15.7%, although the majority of coupons had increases less than 10% as shown in Figure 29. It is important to reiterate that these increases were seen after the coupons were unloaded. Thus, even after the crack had propagated, the electrical resistance was not significantly altered while still under load. Only after returning to the unbent position was the damage evident through higher resistance readings.

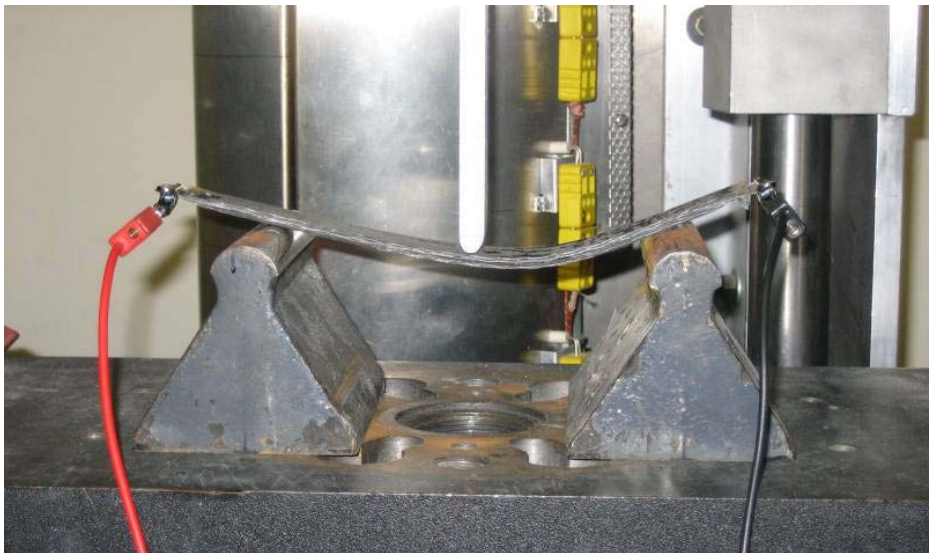

Figure 28. Carbon fiber Mode II resistance testing in bent position.

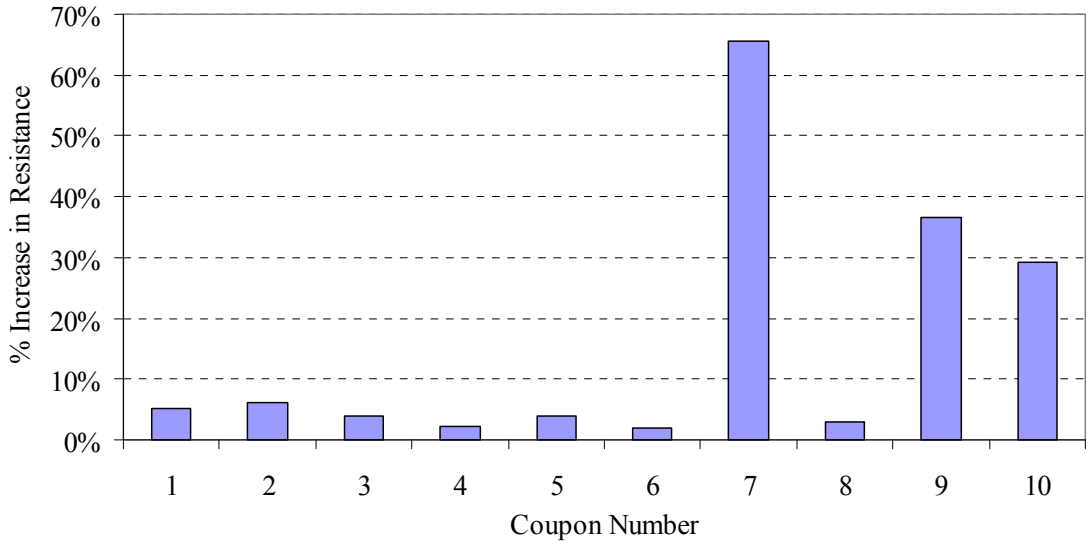

Figure 29. Electrical resistance increases for carbon fiber composite coupons after crack propagation upon unloading.

After experiencing positive results from the carbon fiber composite coupons with CNT reinforcement, those without CNT reinforcement were tested. The first coupon tested was setup with the same geometric parameters and Mode II test speed. However, since the speed was faster than that used in Phase II, the coupon failed through bending in the middle at the point of load application. Another coupon was tested to ensure that these test parameters which worked well for CNT-reinforced coupons were inadequate for those without CNTs. This second coupon failed in the same manner, and as a result the geometric parameters were changed for the rest of the coupons. The remaining eight coupons were tested having an initial crack length of 4 cm, a span length of 15 cm, and width of 2.4 cm.

Again prior to the start of testing, each coupon was measured to determine its resistivity for baseline comparisons. Each of these starting resistance readings can be seen in Appendix A, Section B, which shows a varying degree of starting resistances. For the non-reinforced carbon fiber composite coupons, the initial resistance readings were rather inaccurate and by no means repeatable. Each time the coupons were hooked up to the multi-meter they started at a given value and fluctuated widely. After fluctuating for a time, the resistance readings for all coupons began to steadily increase, due to a capacitive effect. This behavior validated the conductive nature of CNTs, as the composite was much less conductive across the interface when they were not included. In these coupons without CNTs, the resin (non-conductive in nature) greatly affected the resistance. Since the thickness of the layer of resin, compared to that of the surrounding carbon, was thin, the carbon was able to sense some of the electricity being run through the stainless steel. This flow of electricity was then transferred to the resin. The resin was thereby charged by the surrounding carbon, and in essence became a capacitor.

During Mode II testing of these carbon fiber composite coupons without CNTs, resistance readings were recorded manually at 30 second intervals. These values typically started high and as the load was increased, they gradually decreased. For each coupon tested, at a certain point during the Mode II testing, the values became steady and unchanging. These values were extremely low in comparison to the initial fluctuating values experienced prior to testing. The low steady resistance readings were a result of the sample being placed under stress. When placed under stress, the carbon did not

charge the resin layer as it had before. Instead, the resin layer was likely compressed and too thin for the carbon to charge. Hence, the low readings were due to the flow of electricity through the carbon fibers.

When the test was complete, the coupon was left in the bent position and a resistance reading was recorded. Readings taken in the bent position, for all carbon fiber composite coupons without CNTs, were steady (only fluctuating to the tenth of an ohm). These resistance readings were very low compared to the initial readings, and are listed in Appendix A, Section B. Also given are the average resistance values during Mode II testing. When the coupons were released, and returned to a flat position, an additional reading was taken. The resistance for each increased, and then steadily began to climb, again taking on the behavior of a capacitor. The values recorded in the appendix are the values taken upon initially being returned to the flat position. All readings are the baseline from which the resistance started to quickly grow. Thus, unlike the carbon fiber composite coupons with CNTs, these coupons responded poorly to the electrical resistance test. Such electrical resistance testing would not be capable of detecting interfacial damage in the carbon fiber composite without CNTs. Thus, the addition of a CNT layer is necessary for structural health monitoring of the interface using electrical resistance testing, despite the fact that carbon fibers are themselves quite conductive.

To determine the strengthening effects of the CNT layer (and thereby verify the results of previous thesis research), the G_{II} values for both the carbon composites with and without CNTs were calculated. Figures 30 and 31 show each coupon's load versus extension (displacement) graphs used to calculate the required G_{II} values. The two graphs show that carbon fiber composites carry load similarly for both with and without CNTs, however, the crack initiation point for composites with CNTs is delayed. Those coupons with CNTs also were able to reach higher loads before complete failure. This finding was verified by the test results that showed there was an increase in G_{II} for carbon fiber composite coupons with CNTs over that of those without CNTs. Figure 32 displays the normalized average values of G_{II} for Phase III coupons, along with the respective 90% confidence intervals. This comparison indicates that the ten carbon fiber composite coupons reinforced with CNTs had G_{II} values 25% higher (on average) than the eight pure carbon fiber composite coupons. The actual values for each coupon can be seen in

Appendix A, Section C. From this data, it is important to note that each sample set had a similar standard deviation, but the mean values for CNT-reinforced samples were considerably higher and this increase was statistically significant.

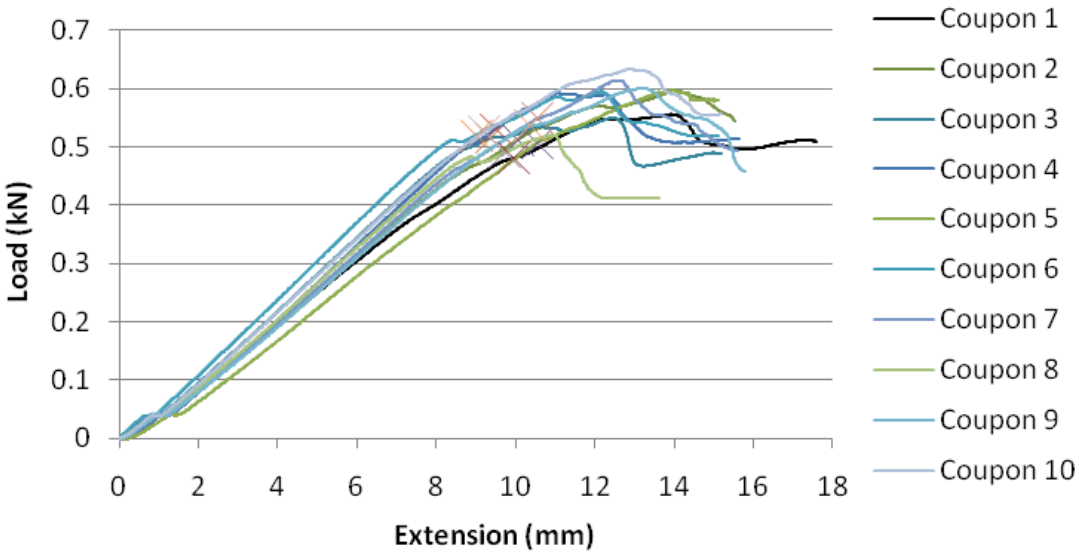

Figure 30. Load-extension data for carbon fiber composites with CNTs.

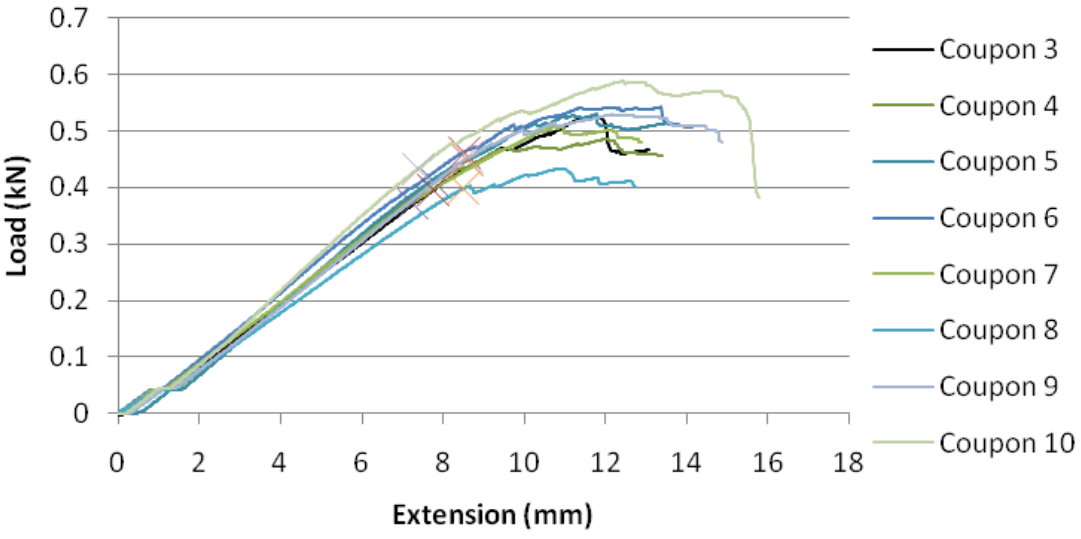

Figure 31. Load-extension data for carbon fiber composites without CNTs.

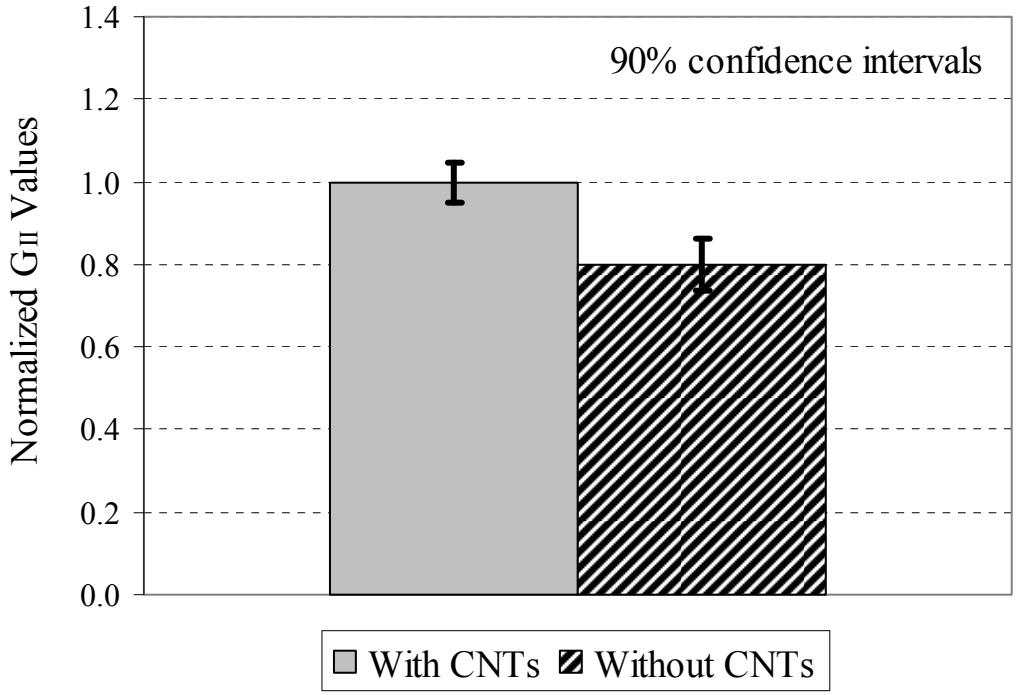

Figure 32. Normalized mean values of G_{II} for carbon fiber coupons with and without CNT reinforcement.

Based on previous Naval Postgraduate School research[26], the layer of CNTs within the carbon fiber composite acted as expected. The coupons without CNTs experienced crack propagation at the initial crack tip, followed by propagation through the joint interface. Coupons with CNTs first experienced cracking at areas away from the crack tip, giving evidence of the strengthening effect of the CNTs along the interface. These cracks then propagated back towards the initial crack tip. These different crack propagations can be verified by observing the surface of the joint interfaces where cracking occurred. Figure 33 shows the relatively smooth joint interface of a coupon without CNTs, with few fibers broken. This is a result of the crack propagating through the joint interface. Figure 34, on the other hand, shows the rougher joint interface of a composite coupon containing CNTs. The rough surface has CNTs on both sides, as well as several areas were the crack propagated back to the initial tip through fibers. The crack was forced to propagate through the fibers due to the CNTs at the joint interface strengthening it and making it resistance to crack propagations.

[26] Faulkner, "Study of Composite Joint Strength with Carbon Nanotube Reinforcement," 27–30.

Figure 33. Crack propagation path of carbon fiber composite without CNTs.

Figure 34. Crack propagation path of carbon fiber composite with CNTs.

D. FIBERGLASS COMPOSITE RESISTANCE TESTING (PHASE IV)

This phase began with Mode II testing of all fiberglass composite coupons containing CNTs. Based on the results of Phase II, the initial crack length was chosen to be 4 cm, with a span length of 16 cm, and width of 2.4 cm. These geometry parameters along with a Mode II test speed of 1 mm/min, resulted in coupon failure through crack propagation rather than due to bending stresses.

Prior to the start of testing each coupon was measured to determine its resistivity for baseline comparisons. Unfortunately, only four of the coupons actually registered any resistance on the multi-meter. An advantage to using fiberglass for testing is that the CNTs inside the fiberglass composite could easily be seen as a black layer along the interface. For the six coupons that did not conduct, gaps within the coupons that were devoid of CNTs were detected as shown in Figure 35. Each of the four coupons that did conduct had a visual path of CNTs that were continuous throughout the entire length of the coupon, as displayed in Figure 36. Thus, in order for CNTs to be effective as a health monitoring sensor in non-conductive media, they must be "touching" within a continuous network. Validation of this continuity is very easy, however, by testing the resistance.

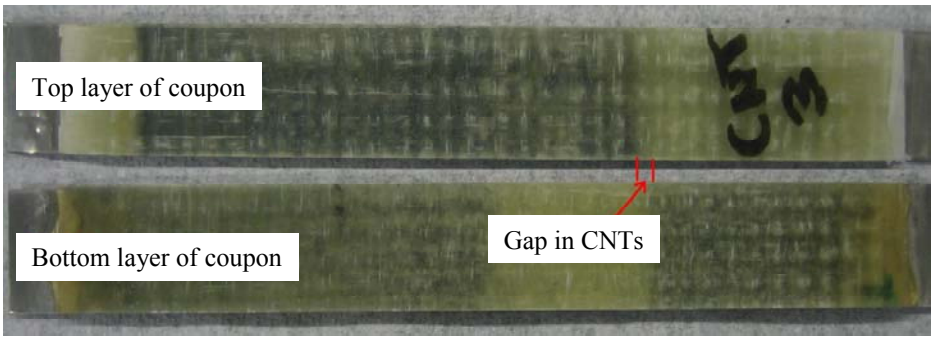

Figure 35. Fiberglass coupon with gap in the layer of CNTs.

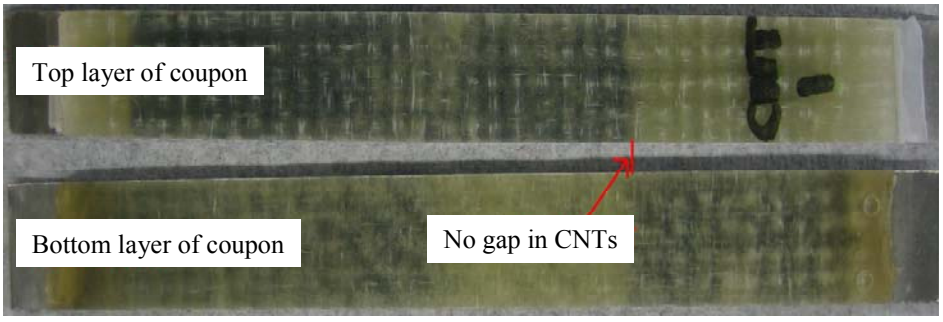

Figure 36. Fiberglass coupon with continuous layer of CNTs.

In order to ensure that CNTs are adequately dispersed, better methods for dispersion during the VARTM process should be investigated. Proper dispersion should result in no open gaps, as experienced in this particular sample set. Optimizing the CNT dispersion was not an objective of this particular project and is left for future study.

Even though only four of the coupons were conductive, all coupons containing CNTs were put through Mode II testing and values of the resistance readings were recorded manually at 30 second intervals. The six coupons that initially did not conduct continued to register no resistance readings during the entire test. The values for the four conducting fiberglass coupons, although much higher than those obtained for the carbon fiber coupons in Phase III, showed the same steady trend. During the test, the resistance readings varied little from the initial readings, and matched within 6%. Even when the sample cracked and continued to crack, the resistance readings stayed constant varying only a few ohms at a time, again consistent with Phase III carbon fiber coupons with CNTs. The average resistance readings during loading for the four conducting coupons are tabulated in Appendix A, Section D.

When the tests were completed, the samples were left in the bent position as done for the carbon fiber coupons. The six coupons that were non-conductive still registered no resistance; however, the remaining four continued to give good resistance readings. The readings in the bent position were constant, but all readings had increased from the initial values, some by as much as 30%. When the coupons were released from this bent position, the resistance readings of these four coupons continued to increase while the non-conducting coupons remained unchanged. Both the bent and flat readings for the four conducting fiberglass coupons are listed in Appendix A, Section D. Although each coupon showed an increase in resistance, some showed higher percentages than others. This variance can be contributed to the CNT dispersion method used during the VARTM process. On average the increase in resistance readings for fiberglass coupons with CNTs was 42.9%. Although much higher, this increase was consistent with increases in carbon fiber composites. The higher values are likely attributable to the less conducting nature of the glass fibers compared to carbon fibers, thus making resistances much higher when the CNT network is disrupted.

Next, the fiberglass coupons without CNTs were tested. These ten coupons each acted as an open circuit before, during, and after Mode II testing, as expected for a non-conductive media. This was exactly how the fiberglass composite samples with gaps in the CNT layers also behaved.

Although previous Naval Postgraduate School showed CNTs could strengthen carbon fiber composites, the Phase IV tests were the first attempt at determining the strengthening capability of CNTs for this type of fiberglass composite. Again, the critical G_{II} values for both the fiberglass coupons with and without CNTs were compared. Test results showed an increase in G_{II} for fiberglass composite coupons with CNTs (9 data points) over that of pure fiberglass coupons (ten data points). Figure 37 displays the normalized average G_{II} values, along with the respective confidence intervals, showing the coupons with CNTs to have G_{II} values 54% higher than those without, with this difference being statistically significant at the $\alpha = 0.05$ level. The actual values for each coupon are tabulated in Appendix A, Section E.

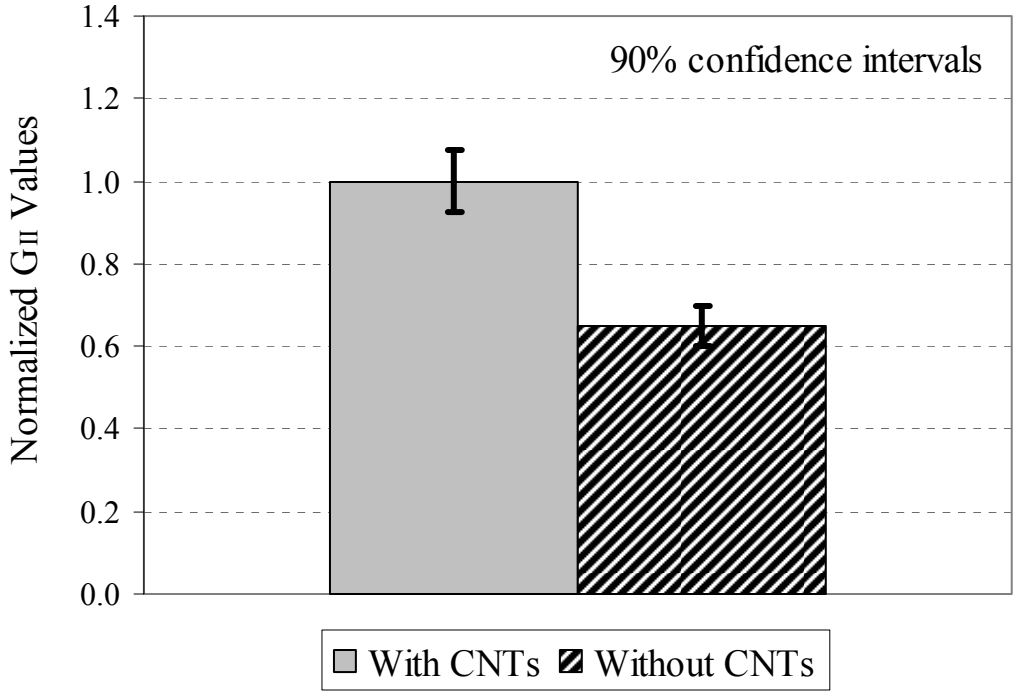

Figure 37. Normalized mean values of G_{II} for fiberglass coupons with and without CNT reinforcement.

Unlike the failure of carbon fiber composite coupons described in the previous section, the fiberglass coupons failed in a more unusual manner. During testing of fiberglass coupons with CNTs, a loud cracking sound could be heard upon failure followed by a quick decrease in the loading. This can be seen in Figure 38, which displays the load versus extension graph for all fiberglass coupons with CNTs. The peak of each graph closely corresponds to the crack propagation point observed visually, audibly, and graphically. This loud cracking sound was not observed during testing of fiberglass composites without CNTs; instead a soft crackling sound could be heard. Also with the pure fiberglass coupons, after the crack could be visually and audibly verified, loads being applied still continued to climb. This can be shown in Figure 39, which also displays the location where the crack could be seen and heard.

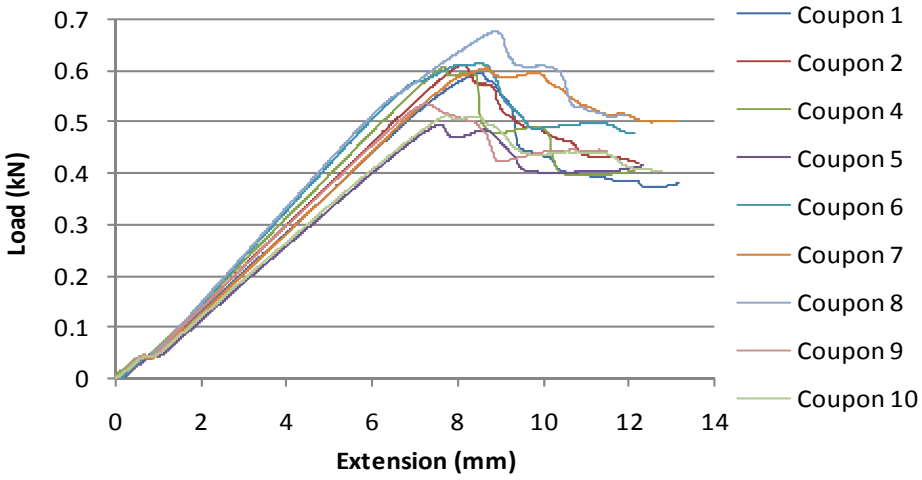

Figure 38. Load-extension data for fiberglass coupons with CNTs.

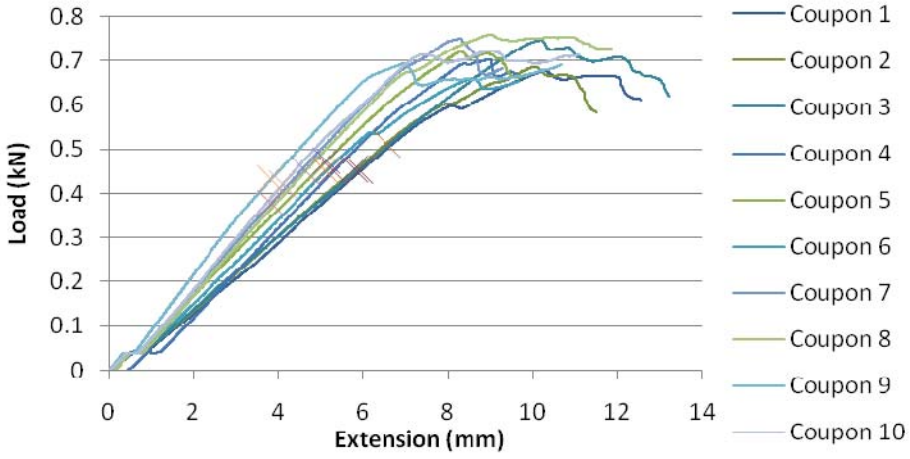

Figure 39. Load-extension data for fiberglass coupons without CNTs.

Differences in both the sound of failure, and crack propagation can be directly attributed to the CNTs. In the non-reinforced samples, crack propagation began at the tip of the initial crack, and continued to propagate through the joint interface, as shown in Figures 40 and 41. This crack occurred early in the loading cycle and slowly propagated while still maintaining an increasing load. For the fiberglass composites reinforced with CNTs, they too initially propagated from the crack tip through the joint interface. However, at a certain point the crack took the path of least resistance under the layer of CNTs, as shown in Figures 42 and 43. This result was widely observed in the CNT-reinforced samples, and was the source of the loud cracking sound.

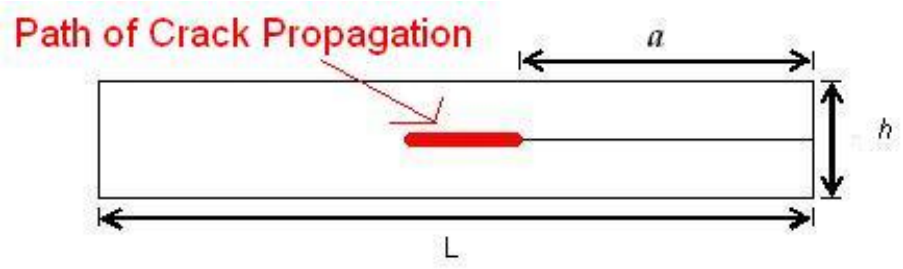

Figure 40. Path of crack propagation in fiberglass coupons without CNTs.

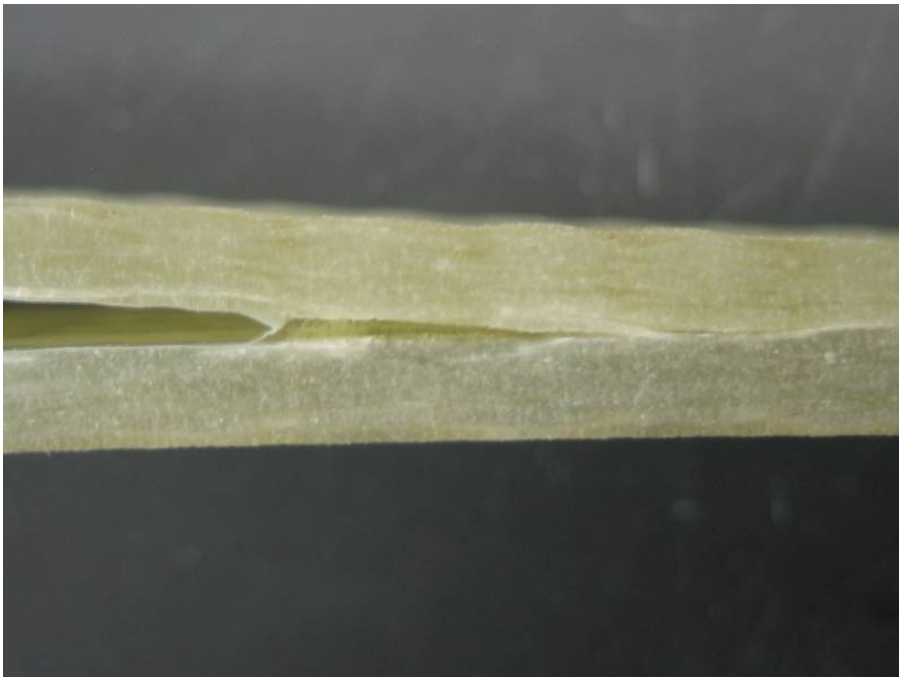

Figure 41. Crack propagation image for fiberglass coupon without CNTs.

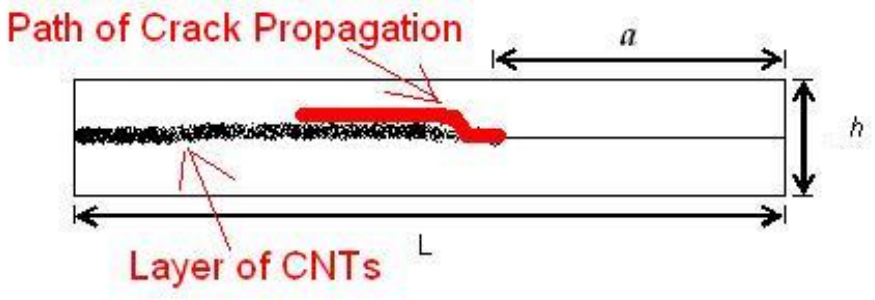

Figure 42. Path of crack propagation in fiberglass coupons with CNTs.

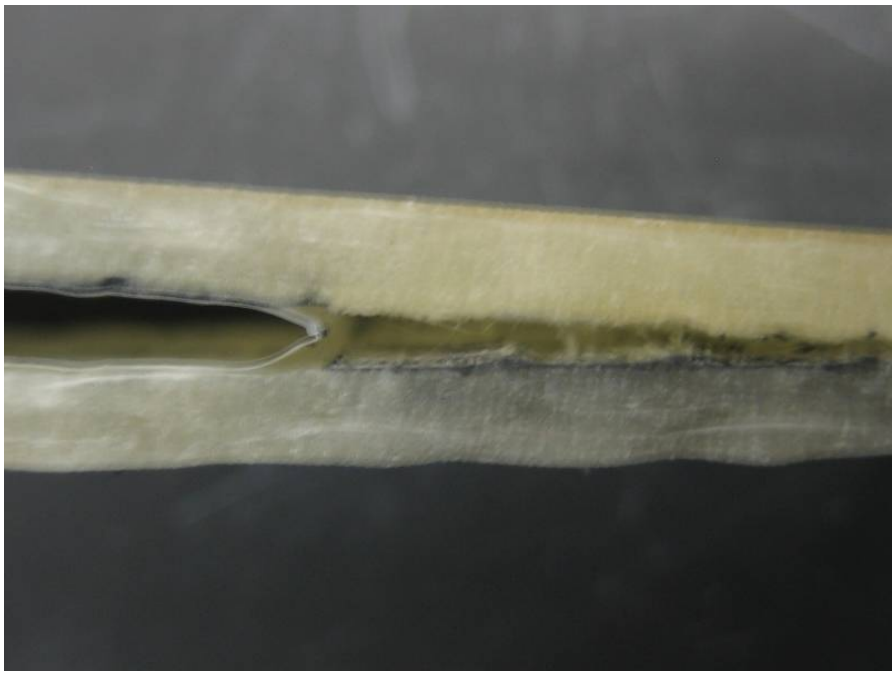

Figure 43. Crack propagation image for fiberglass coupon without CNTs.

After all testing was completed, coupons in which crack propagation occurred were pulled apart to inspect the cracked joint interface surface, and verify crack propagation paths. When the fiberglass coupons with CNTs were pulled apart, one side contained more CNTs than the other. Looking closer, it could be seen that initially the crack did propagate through the layer of CNTs, but then quickly took the path of least resistance under the layer of CNTs through the fiberglass. The fiberglass coupon without CNTs showed a slightly different crack propagation path. The joint interface bond was broken through the resin by the crack propagation, resulting in the resin being pulled away from the fibers. Both surface interfaces are shown in Figures 44 and 45.

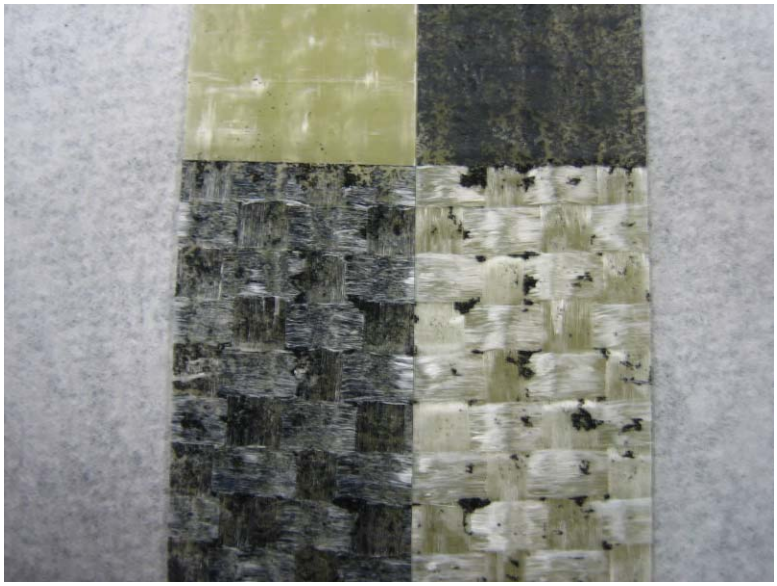

Figure 44. Surface view of crack propagation path in fiberglass coupon with CNTs.

Figure 45. Surface view of crack propagation path in fiberglass coupon without CNTs.

The differences in crack surfaces can also explain the differences in the physical observations, as well as the differences in the loads each sample set was able to carry. The pure fiberglass composite acted as the two-step cured samples tested during Phase II. The crack propagated through the joint interface, an area which was inherently stronger due to the VARTM process. This allowed for higher loads to be carried and slower crack growth. The fiberglass without CNTs acted more like the co-cured samples from Phase

II. Once the crack propagated into layers above or below that of the CNTs, it was propagating through a weaker resin bond allowing faster crack propagation and lower loads to be carried. This is likely why, although crack propagation was prolonged in the fiberglass with CNTs, those without were still able to carry higher loads.

E. RESISTANCE RELIABILITY AND CRACK GROWTH RELATIONSHIP TESTING (PHASE V)

This phase began with testing of the four fiberglass composite coupons containing CNTs, from Phase IV, for which resistance readings were able to be obtained. All coupons tested were placed on the Instron with the same test setup from Phase III and IV. Thus, a span length of 16 cm and width of 2.4 cm were still used. Before placing the coupons into the machine, however, the lengths of the cracks resulting from Phase IV Mode II tests were measured and recorded. Once loaded into the Instron, a load of 100 kN was applied to the coupons such that the crack was stationary without growth and the corresponding resistance readings were taken for both bent and unbent readings. This was done at least three times for each sample. The resulting resistance readings are tabulated in Appendix A, Section F.

Although the readings varied from the cracked resistance readings taken in Phase IV (as shown in Appendix A, Section D), each coupon was consistent in itself, only varying by at most 6.35%. Again the differences between the coupons can be attributed to the uneven distribution of CNTs within the coupons. The readings also varied from those taken in Phase IV due to the slightly different location point where the multi-meter was attached to the sample. In future applications, the exact location of the test equipment should be marked in order to ensure consistent readings from one test to the next, as it was shown that the exact location of the contact points had some noticeable effect on measurements.

After taking the consistency readings, the fiberglass coupons were then manually loaded for crack growth using the Instron machine. Unfortunately, no useful information was gathered from this step. Upon crack propagation, resistance readings jumped to over 1 MΩ. These high readings were indications that the CNTs were no longer touching and the sample was now acting as an open circuit. In essence, the crack had severed the

continuous layer of CNTs and began to propagate below the layer of CNTs. This is what was observed and discussed in the Phase IV results when the samples were pulled apart for inspection.

The same type of tests were then conducted using all carbon fiber composite coupons containing CNTs from Phase III. The same geometry was used, and the lengths of the cracks resulting from previous Mode II tests during Phase III were measured and recorded. This time a load of 50 kN was applied to the coupons. The corresponding resistance readings for both the bent and unbent positions were taken. This was done at least three times for each sample. The resulting resistance readings are tabulated in Appendix A, Section G.

As with the fiberglass composites, the readings for the carbon fiber composites were consistent for each coupon. The average change in resistance was 1.26% with the highest resistance change being 8.77%. Any difference between the coupons can be attributed to the uneven distribution of CNTs within the coupons. As was seen with the fiberglass, the resistance of carbon fiber coupons also varied from those measurements taken in Phase III. As already discussed, this is due to the different placement of where the multi-meter was attached to the sample.

After taking the consistency readings, the carbon fiber coupons were then manually cracked using the Instron machine. Once the crack propagated, which was determined by both sight and sound, the new crack length was measured, and the corresponding resistance reading was taken. This was done repeatedly until the crack tip had reached the point of load application, and it was no longer possible to further crack the coupons with the Instron machine. The resulting data was then plotted to determine the relationship between change of crack length and change in resistance. Figure 46 shows all the data collected for coupons with CNTs on the same graph.

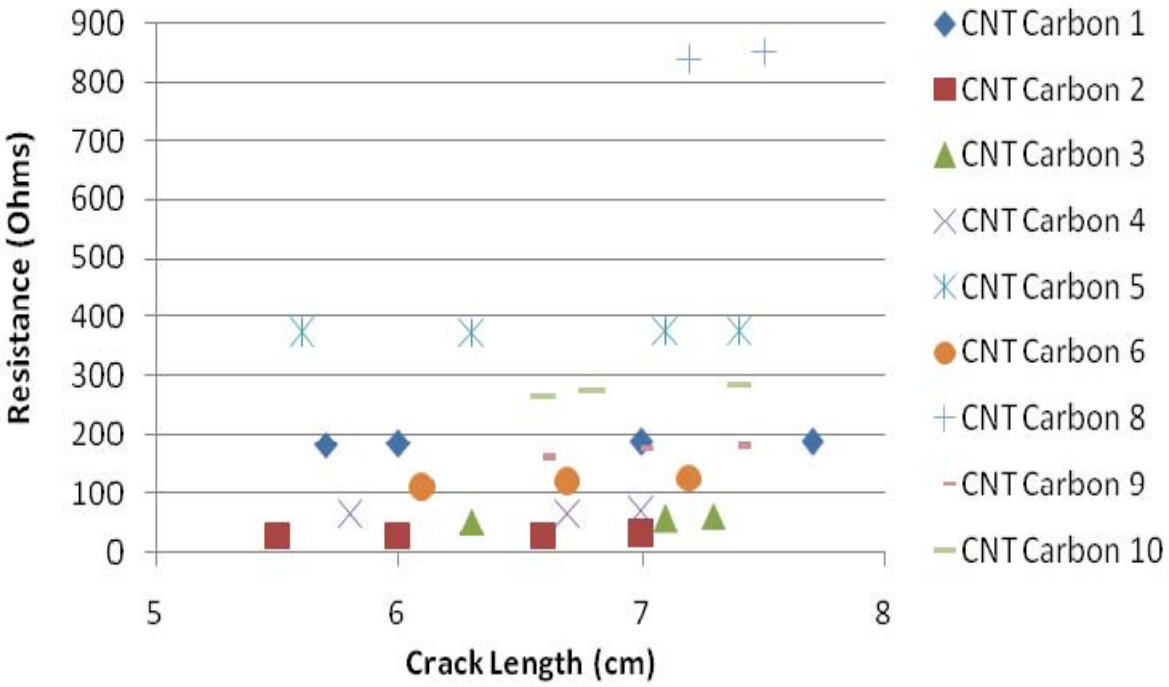

Figure 46. Resistance vs. crack length for all carbon fiber coupons with CNTs.

Because the resistance readings from coupon to coupon vary due to unique CNT dispersions, it's useful to see the trends in resistance versus crack length for individual coupons, and determine if these trends follow similar relationships. The nine figures which follow Figures 47 through 55) show the same data as in Figure 46, but data for each coupon are plotted separately. The electrical resistance varied approximately linearly with crack length for those samples with four data points, as these figures show. A least-squares linear regression line is shown for each, even if there were less than four data points. These figures show that no standard slope fits each plot, although an average value was taken to be 13.68 ohms/mm with a standard deviation of 14.52 ohms/mm. The fact that each plot of resistance versus crack length has a different slope presents a challenge to the use of dispersed CNTs as a means for damage progression. It appears that it is very important to make the CNT networks as uniform as possible. In addition, calibration for each specimen may be required.

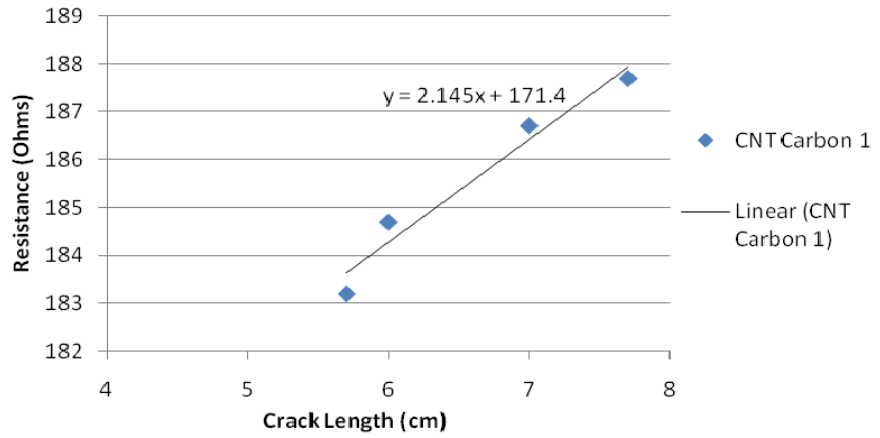

Figure 47. Electrical resistance vs. crack length, carbon fiber coupon #1.

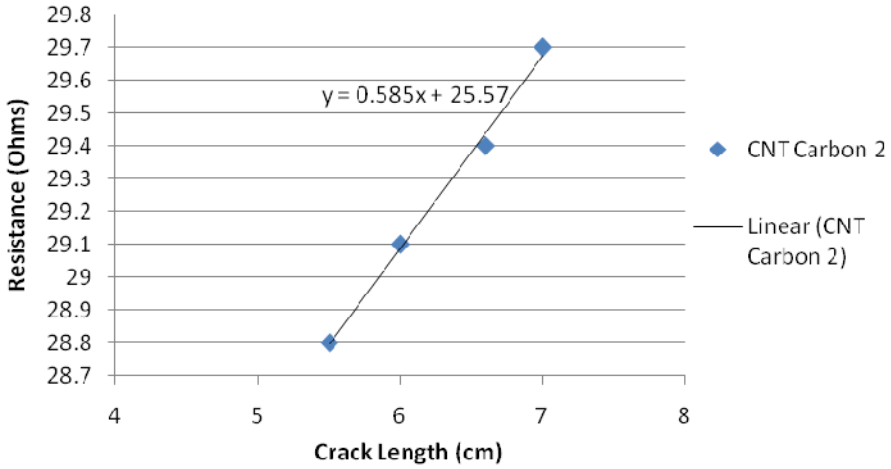

Figure 48. Electrical resistance vs. crack length, carbon fiber coupon #2.

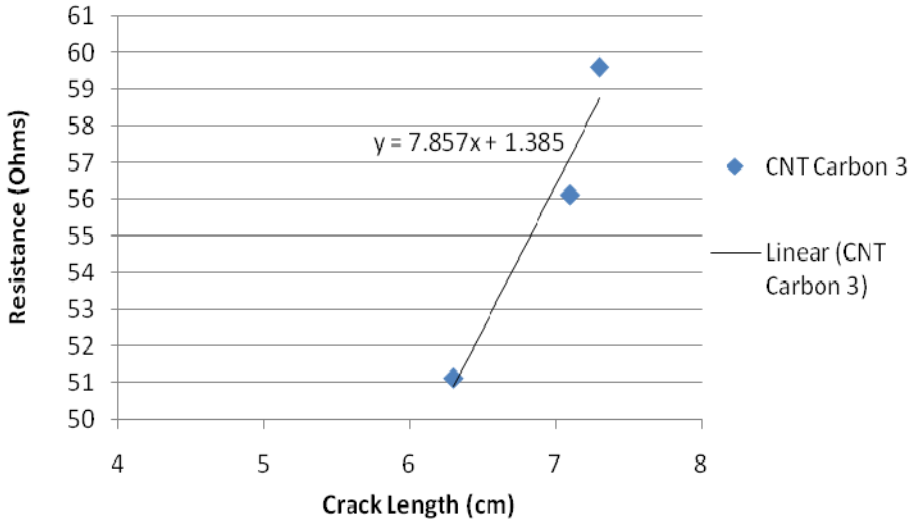

Figure 49. Electrical resistance vs. crack length, carbon fiber coupon #3.

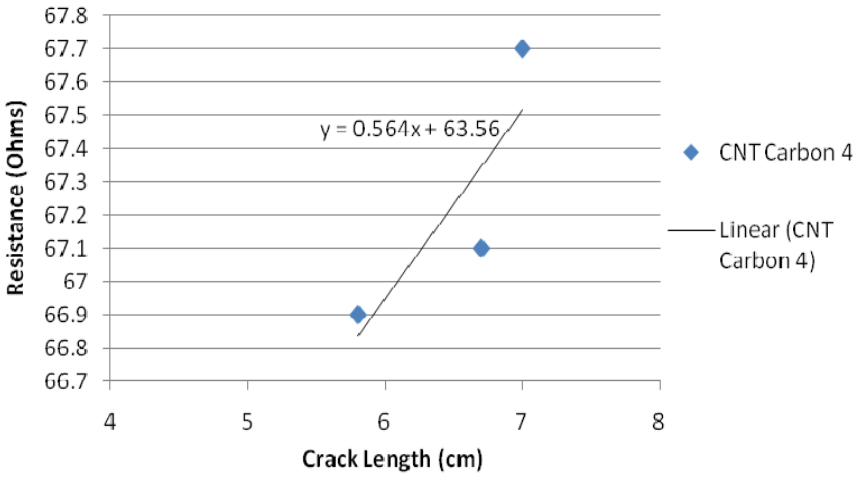

Figure 50. Electrical resistance vs. crack length, carbon fiber coupon #4.

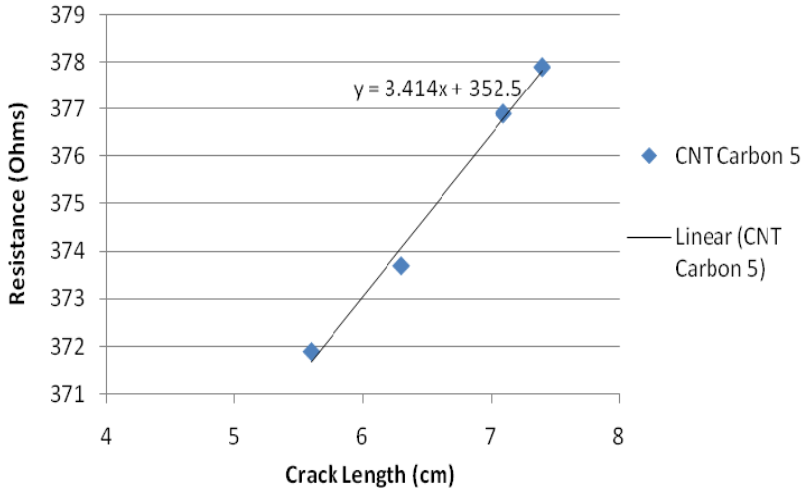

Figure 51. Electrical resistance vs. crack length, carbon fiber coupon #5.

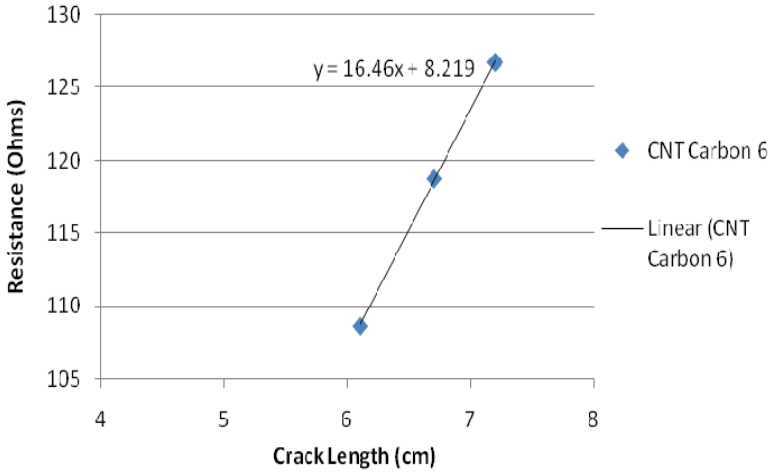

Figure 52. Electrical resistance vs. crack length, carbon fiber coupon #6.

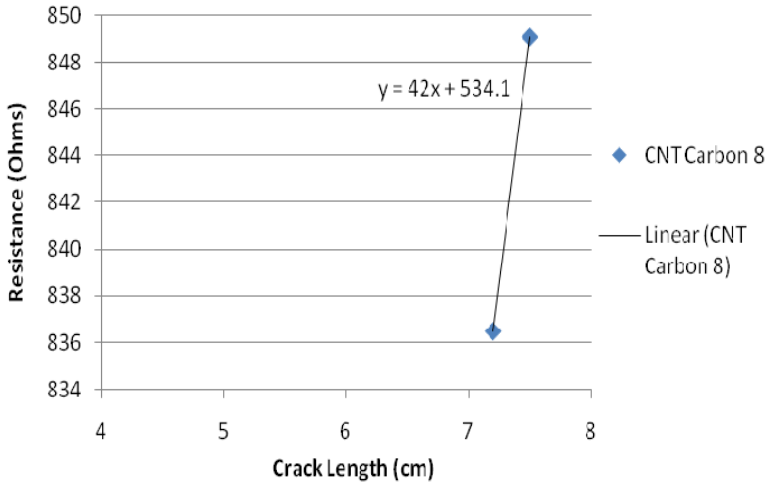

Figure 53. Electrical resistance vs. crack length, carbon fiber coupon #8.

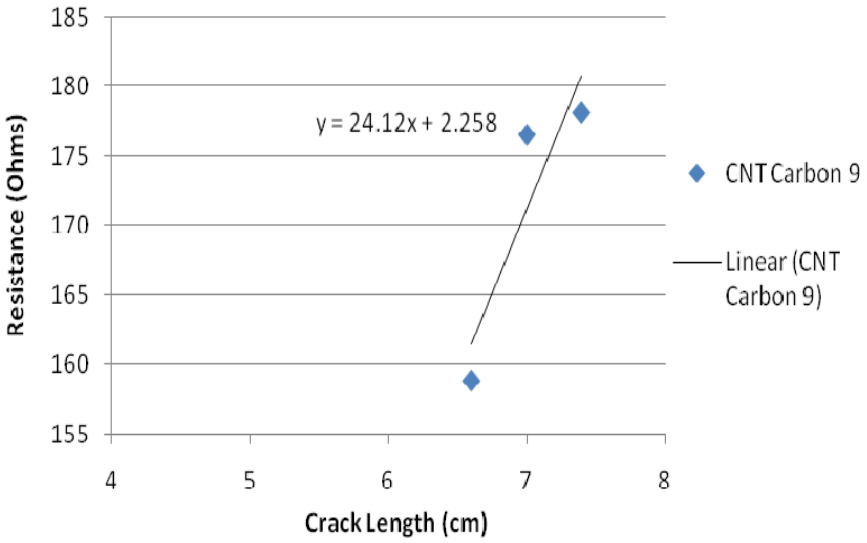

Figure 54. Electrical resistance vs. crack length, carbon fiber coupon #9.

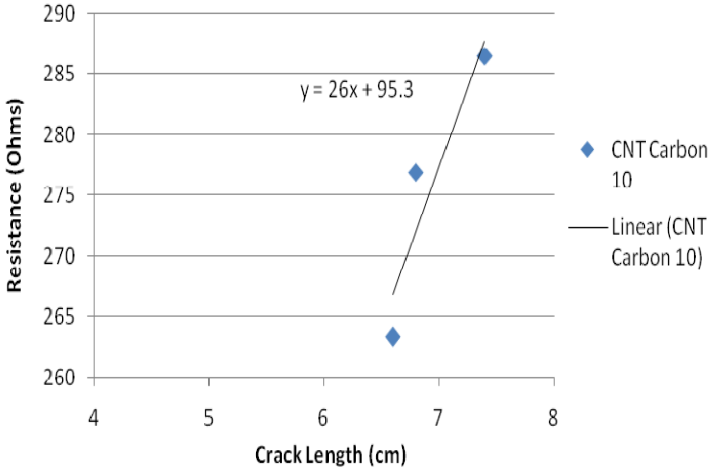

Figure 55. Electrical resistance vs. crack length, carbon fiber coupon #10.

These figures appear to have similar general trends independent of the starting crack length and initial resistance reading. With each incremental increase in crack length, the resistance values increased. Although it was difficult to predict how much the crack would propagate each time it was loaded, the resistance never failed to increase, even with the smallest increase in crack length. This increase in resistance is related to the fact that the cracks for carbon fiber coupons with CNTs propagated through the layer of CNTs. Thus, as the crack continued to propagate, the CNTs were separated from each other, and their ability to conduct throughout the sample decreased. The more holes in the layer of CNTs, the harder it is to conduct, and thus an increase in resistance.

Although there seems to be a linear relationship, more testing needs to be done to verify these findings. More data points need to be taken in order to truly determine if a linear relationship is the correct one to assign to the resistance behavior of CNTs dispersed along composite interfaces. For future work, this data could be improved by ensuring a more even dispersion of CNTs, designated test equipment positions for the multi-meter, and using a more rigorous method to predict crack propagation in intermediate steps.

THIS PAGE INTENTIONALLY LEFT BLANK

VI. CONCLUSIONS

In summary, interface strength of woven fabric composite layers was studied using Mode II fracture strength testing. Both carbon fiber and E-glass fiber composites were used with the vinyl ester resin. These composites were fabricated using the VARTM process. The project consisted of five experimental phases. The first phase was merely a familiarization phase to allow the student researcher to gain proficiency in constructing and testing composite samples. Next, the co-cured composite interface strength of carbon fiber composite samples was compared to that of the two-step cured interface as used, for example, in the scarf joint technique. The test results showed that the two-step cured interface was as strong as the co-cured interface. This finding is significant in that it suggests that a two-step curing process does not diminish fracture properties compared to co-curing, allowing the use of a two-step curing process for modular construction or repair of large structures. In addition, two-step curing may more easily enable the application of carbon nanotubes to the interfaces where reinforcing materials such as fibers are discontinuous, especially if VARTM is used as the assembly process. It is important that the use of two-step curing does not diminish the very properties the addition of carbon nanotubes is meant to improve.

The next two sets of tests were focused on the application of carbon nanotubes to the composite interface using the two-step curing technique. One set of tests was conducted using carbon fiber composite samples, while the other set of tests used E-glass fibers. For each material, Mode II fracture testing was accomplished on samples containing CNTs dispersed along the interface, as well as samples without the addition of CNTs. The results indicated a significant improvement of the interface fracture toughness due to CNTs for both the carbon fiber and fiberglass composites. The carbon fiber samples showed a 25% improvement in Mode II critical strain energy release rate with the addition of CNTs compared to the baseline without CNTs. Likewise, the increase was 54% for the fiberglass samples. These results validate previous Naval Postgraduate School research with carbon fiber composites which showed that Mode II fracture properties can be significantly improved by adding a dispersed CNT layer along critical interfaces where failure is matrix dominated.

Lastly, the final phase of research focused on the ability to detect interface crack growth using the CNTs introduced at the interface. Because CNTs have high electrical conductivity, the electrical resistance was measured through the interface during Mode II loading which induced crack propagation. For fiberglass coupons, only the initial crack propagation was detected through increased resistance because the interface was so strengthened by the addition of CNTs that the crack actually propagated below the CNT layer after breaking through the fibers. This led to an open circuit condition once the crack propagated. This is not a discouraging result by any means, as the normally non-conductive fiberglass material was conductive before loading with the CNT layer added, and crack growth was then associated with a large increase in resistance. Thus, the CNT layer both strengthened the interface and provided means of determining when crack propagation occurred.

In the carbon fiber samples, however, the crack propagated along the interface as loading increased, and a gradual increase of electrical resistance was observed as a function of crack length. As a result, the change of electrical resistance in terms of crack length change could be studied for carbon fiber samples. It appears that a linear relationship exists between electrical resistance and crack length for these carbon fiber samples. However, because the distribution of CNTs was unique for each coupon, the actual values of resistance and the slope of the resistance vs. crack length curve was different for each sample. This result is not surprising, and indeed was as expected since the electrical conductivity is based on the distribution of the CNT network. Ensuring a more uniform distribution is certainly possible compared to the manual means used for this testing, but the VARTM process and the nanoscale network of the CNTs both make the repeatability of uniform dispersion a difficult task. Uniformity can be improved but never truly attained. This limitation has practical significance as it may be difficult or impossible to determine crack length (and thus predict when failure will occur) based on electrical resistance measurements alone. However, if resistance can be shown to vary roughly linearly with crack length (or in some other known fashion), then it may be practical to use resistance measurements to determine crack length if the two are correlated using a crack length measurement. For example, if the resistance increased 5 ohms while the flaw size increased 5 mm for a particular joint, then future electrical

resistance increases could be expected to increase 1 ohm for every 1 mm crack length growth. The necessity of such correlation may make the use of embedded CNT layers more advantageous when combined with other non-destructive evaluation techniques, rather than used as a stand-alone means for structural health monitoring.

One important point regarding the use of electrical resistance measurements to detect damage is that the resistance increases observed in this study tended to occur after the specimens which cracked were unloaded. Thus, while the specimens were still in the bent position, it was more difficult to detect whether they had cracked using electrical resistance. But once they returned to their unbent position, resistances were higher if cracking had occurred. This result suggests that electrical resistance measurements should be compared when the interface is under no load (or a constant baseline load) to determine the extent of damage, rather than measure and compare the resistance while under load to that before loading.

This phenomenon also led to the speculation that the increasing resistance could be more due to straining and unstraining of the CNT layer rather than propagation of the interfacial crack. For this reason, the additional tests were conducted in which precracked specimens were loaded without further crack propagation, with resistance measured before, during, and after loading. The increases in resistance were generally very small if no further cracking occurred. Thus, it appears that electrical resistance increases were more associated with crack propagation and not with disruption of the CNT layer for loads in which no crack propagation occurred. But it is important to note that such small increases under loads without crack propagation may become less insignificant if more and more load cycles were to be applied. For this project, many cyclic loads were not considered. A follow-on study should investigate the effect of repeated load cycles on the CNT layer's resistance for loads at which macroscopic crack propagation does not occur. This analysis would be useful in determining if the electrical resistance of the CNT layer is stable enough under load cycles to be useful for damage monitoring, or whether it is overly sensitive so that a large number of false positives may occur when cracks have not reached critical stages.

Although there is much work yet to be done to make the use of CNT layers a practical means for structural health monitoring of key interfaces, there are two key takeaways from this study: (1) the use of CNTs significantly improved the Mode II fracture properties along interfaces for two different composites of military importance, and (2) the electrical resistance of the CNT layers within these composites increased as damage progressed at the interface. These two results suggest the promise of CNTs for health monitoring of critical interfaces in composite structures. Avenues for further study are discussed in the next chapter.

VII. RECOMMENDED FURTHER STUDY

This chapter recommends further research to advance the capability of carbon nanotube networks to both strengthen key interfaces while providing means of damage detection through electrical resistance measurements. There are three primary thrusts which are proposed for further study:

1. Investigation of the electrical conductivity enhancement of carbon nanotube networks in composite media at both the nanoscale and macroscale.
2. Investigation of the efficacy of carbon nanotube networks to improve strength properties and provide damage detection capability in composite interfaces of military significance.
3. Development of a structural health monitoring prototype incorporating a carbon nanotube network in a composite structure under representative loading.

Each of these areas are discussed in more detail in the paragraphs below.

A. INVESTIGATION OF THE ELECTRICAL CONDUCTIVITY OF CNT NETWORKS AT BOTH THE NANOSCALE AND MACROSCALE

This area of proposed research should build on some of the recent study to better understand the mechanisms of electrical conductivity enhancement of CNT networks in solid media, particularly those networks dispersed along interfaces within composite materials. A more fundamental understanding of these mechanisms allows better modeling of CNT networks for structural health monitoring applications. The insights derived from such modeling can reduce the dependence on experimental exploration, better focus experimental study using the most promising design parameters, and validate experimental results. If the interaction of CNTs with matrix and/or adhesive material can be better understood at the nanoscale, such information may better predict results at the macroscale using such techniques as multiscale numerical simulation.

There are a large number of design parameters which have yet to be adequately studied. Investigation of these design parameters may be best approached initially using an experimental strategy utilizing a design of experiments methodology to characterize

CNT networks based on those properties which are deemed the most desirable. Examples of such desirable properties may include sensitivity of the network's electrical resistance to damage, stability of resistance measurements to load cycles without damage, ability to be dispersed uniformly, and cost. Possible design parameters are listed below.

- The type of CNTs used (e.g., single-walled, double-walled, multi-walled; a combination thereof; or more complex geometries)
- The length and aspect ratio (length to diameter) of CNTs
- The surface concentration of dispersed CNTs
- The type of dispersant used to distribute the CNT network
- The use of functionalization (i.e., the addition of side groups to the outer CNT wall through chemical treatment) to prevent CNT clustering
- The type of matrix and/or adhesive materials
- Fabrication technique and related process variables

It is certain that no single combination of design parameters will be ideal for all applications, and thus a representative baseline (or baselines) should be established for which such study can initially be focused. Lessons learned from this baseline configuration can then be exploited in the next recommended area of study. One example of recent Naval Postgraduate School in this area is the investigation of CNTs to improve the mechanical properties of adhesive joints.[27] It was found that the type, size, and functionalization (in this study, carboxyl side groups were used) of the CNTs played a very significant role in improving the joint strength of steel-composite and composite-composite adhesive joints. While some design parameter settings significantly improved the joint strength under Mode II loading, others reduced strength. These findings are consistent with previous Naval Postgraduate School experimental work. Thus, it is not as simple as "add CNTs, improve mechanical properties."

[27] Garrett L. Burkholder, *The Effects of Carbon Nanotube Reinforcement on Adhesive Joints for Naval Applications,* Naval Postgraduate School, MS thesis, December 2009.

B. INVESTIGATION OF THE EFFICACY OF CNT NETWORKS TO IMPROVE STRENGTH AND MONITOR DAMAGE PROGRESSION

The objective of this area of research would be to further evaluate the use of CNT networks (and/or other nanoparticles or nanofibers) as a means to strengthen and monitor composite joints of military interest. A basic research strategy should ideally include the following general tasks:

1. Experimental study of interface strength with added nanoparticles/nanofibers.
2. Numerical modeling (based on first principles or empirical relationships) of interface strength with added nanoparticles/nanofibers.
3. Experimental study of progressive damage monitoring of composite interfaces.
4. Numerical modeling (based on first principles or empirical relationships) of progressive damage monitoring of composite interfaces.

The interface(s) under study should be chosen based on relevance to the sponsoring agency. Types of interfaces include the inter-layers of laminated composite plates, scarf joint interfaces, the skin-core interfaces of sandwich composites, and adhesive layer interfaces. The tests reported in this technical report focused solely on crack propagation under Mode II loading in a three-point bend test. Other modes of failure should also be addressed, to include Mode I, Mode II, and mixed Mode I/II crack propagation under both static and dynamic loads. In addition, effects of cyclic loading on the stability of electrical resistance measurements across the nanoparticle/nanofiber layer should be investigated to ensure resistance increases correspond to actual physical damage rather than progressive load cycles. The insights gained from the proposed research in the previous section would be very useful in setting design parameters, such as the type, size, and surface concentration of nanoparticles. However, a detailed study of electrical conductivity mechanisms and influence of design parameters is not necessarily a prerequisite to experimental testing and empirically-based numerical simulations.

C. DEVELOPMENT OF A STRUCTURAL HEALTH MONITORING PROTOTYPE BASED ON A CNT NETWORK

The final area of proposed study focuses on the development of a laboratory prototype structural health monitoring system utilizing a CNT network (or other nanoparticle/nanofiber). The objective is to demonstrate the feasibility of simultaneously strengthening and monitoring a critical interface using nanotechnology. To this point, the proposed research focused on better understanding of the strengthening and conductivity effects of nanolayers in composite materials. This phase of research would utilize these findings for one or more interfaces (preferably both simple in design and relevant to real-world applications). The tasks required would likely include the following:

1. Fabricate a component which requires health monitoring of a critical interface (or interfaces) with and without CNT reinforcement.
2. Subject the component to representative loads (static, dynamic, and cyclic) and measure electrical resistance across the interface as damage progresses.
3. Calculate and compare strength characteristics, and correlate electrical resistance values to physical damage progression.
4. Develop a structural health monitoring algorithm to assess damage and predict residual strength and/or life based on status of damage.
5. Construct a new set of components with CNT reinforcement and subject them to similar loads, using the reasoning algorithm to predict residual strength and life based on damage monitoring.
6. Compare predictions to actual performance and improve as necessary.

Based on both F/A-18 and 787 Dreamliner delamination issues near the wing root, a suggested scenario could be a slender component subjected to flexural stresses (static, dynamic/impact, and cyclic) for either a composite plate adhesively bonded to a metal root, a composite stiffener bonded to a metallic skin, a sandwich composite plate, or a laminated composite plate.

All three of the proposed research areas could be concurrent areas of study, with cross-flow of lessons learned and insights.

APPENDIX A. TEST DATA TABLES

A. TWO-STEP CURED AND CO-CURED CRITICAL STRAIN ENERGY RELEASE RATES

Two-Step Cured						
Sample	G_{IIC} (N/m)	C (m/N)	P_c (N)	L (cm)	a (cm)	b (cm)
2D	1.016E+03	9.4697E-06	713.901	6.5	2.6	2.40
2E	9.533E+02	8.6957E-06	721.556	6.5	2.6	2.40
2G	6.521E+02	6.7340E-06	608.57	6.0	2.6	2.40
2H	7.168E+02	7.0771E-06	643.331	6.0	2.5	2.40
2I	6.745E+02	9.2507E-06	545.831	6.0	2.5	2.40
Co-Cured						
Sample	G_{IIC} (N/m)	C (m/N)	P_c (N)	L (cm)	a (cm)	b (cm)
1C	8.905E+02	1.0905E-05	584.557	6.5	2.8	2.40
1D	8.741E+02	1.1186E-05	589.716	6.5	2.7	2.40
1E	8.850E+02	1.1236E-05	592.069	6.5	2.7	2.40
1F	5.933E+02	9.0909E-06	534.883	6.0	2.4	2.40
1G	6.372E+02	9.2851E-06	512.308	6.0	2.6	2.40
1H	7.500E+02	9.7182E-06	511.263	6.0	2.8	2.40

B. RESISTANCE MEASUREMENTS FOR CARBON FIBER COMPOSITES WITH AND WITHOUT CNT REINFORCEMENT

With CNTs					
Sample Number	Initial Resistance (Ohms)	Average Resistance During Testing (Ohms)	Resistance in Bent Position (Ohms)	Resistance in Flat Position (Ohms)	Percent Increase in Resistance
1	173.3	173.1	173.5	182.2	5.14%
2	26.5	26.5	26.9	28.1	6.04%
3	49.3	49.2	49.2	51.2	3.85%
4	71.6	71.6	71.1	73.1	2.09%
5	232.5	234.9	235.2	241.4	3.83%
6	287.2	286.4	277.6	293.1	2.05%
7	74.5	85.2	75.2	123.4	65.64%
8	1081.0	1043.5	1046.0	1112.0	2.87%
9	455.6	281.1	148.5	622.8	36.70%
10	252.5	300.1	288.8	326.2	29.19%
Average	270.4	255.2	239.2	305.4	15.7%
Without CNTs					
Sample Number	Initial Resistance (Ohms)	Average Resistance During Testing (Ohms)	Resistance in Bent Position (Ohms)	Resistance in Flat Position (Ohms)	Percent Increase in Resistance
1	91.25	25.93	16.61	76.60	-16.05%
2	9.16	4.27	3.67	6.23	-31.99%
3	1750.00	322.15	8.75	5500.00	214.29%
4	9.73	7.50	7.94	9.82	0.92%
5	18.10	10.64	5.05	18.10	0.00%
6	35.30	9.71	10.80	38.40	8.78%
7	453.00	8.82	5.21	71.30	-84.26%
8	435.20	58.56	4.30	454.00	4.32%
9	230.00	6.37	4.55	59.50	-74.13%
10	17900.00	23.00	7.25	1270.00	-92.91%
Average	2093.17	47.69	7.41	750.40	-7.10%

C. CRITICAL STRAIN ENERGY RELEASE RATES FOR CARBON FIBER COMPOSITES WITH AND WITHOUT CNT REINFORCEMENT

With CNTs						
Sample	G_{IIC} (N/m)	C (m/N)	P_c (N)	L (cm)	a (cm)	b (cm)
1	1.069E+03	1.8797E-05	480.229	8.0	4.0	2.40
2	1.161E+03	1.7953E-05	512.076	8.0	4.0	2.40
3	1.056E+03	1.6129E-05	515.066	8.0	4.0	2.40
4	1.103E+03	1.5898E-05	530.225	8.0	4.0	2.40
5	1.208E+03	1.9084E-05	506.515	8.0	4.0	2.40
6	1.023E+03	1.5361E-05	519.672	8.0	4.0	2.40
7	1.272E+03	1.7123E-05	548.763	8.0	4.0	2.40
8	9.998E+02	1.6835E-05	490.636	8.0	4.0	2.40
9	1.244E+03	1.7483E-05	537.113	8.0	4.0	2.40
10	1.116E+03	1.6367E-05	525.651	8.0	4.0	2.40
Without CNTs						
Sample	G_{IIC} (N/m)	C (m/N)	P_c (N)	L (cm)	a (cm)	b (cm)
3	8.392E+02	1.8519E-05	395.551	7.5	4.0	2.40
4	8.207E+02	1.6892E-05	409.557	7.5	4.0	2.40
5	9.486E+02	1.6313E-05	448.06	7.5	4.0	2.40
6	1.045E+03	1.6892E-05	462.116	7.5	4.0	2.40
7	7.502E+02	1.8692E-05	372.25	7.5	4.0	2.40
8	9.106E+02	1.9920E-05	397.264	7.5	4.0	2.40
9	1.042E+03	1.7483E-05	453.597	7.5	4.0	2.40
10	8.431E+02	1.5504E-05	433.296	7.5	4.0	2.40

D. RESISTANCE MEASUREMENTS FOR FIBERGLASS COMPOSITES WITH CNT REINFORCEMENT

With CNTs					
Sample Number	Initial Resistance (Ohms)	Average Resistance During Testing (Ohms)	Resistance in Bent Position (Ohms)	Resistance in Flat Position (Ohms)	Percent Increase in Resistance
1	38,120	38,572	39,950	44,550	16.87%
2	357,100	336,850	404,100	455,300	27.50%
4	73,090	74,531	88,100	146,500	100.44%
7	717,600	742,434	939,200	909,200	26.70%
Average	296,477	298,096	367,837	388,887	42.9%

E. CRITICAL STRAIN ENERGY RELEASE RATES FOR FIBERGLASS COMPOSITES WITH AND WITHOUT CNT REINFORCEMENT

With CNTs						
Sample	G_{IIC} (N/m)	C (m/N)	P_c (N)	L (cm)	a (cm)	b (cm)
1	9.803E+02	1.3106E-05	550.607	8.0	4.0	2.40
2	1.109E+03	1.2516E-05	599.307	8.0	4.0	2.40
4	1.054E+03	1.2063E-05	595.245	8.0	4.0	2.40
5	7.802E+02	1.3986E-05	475.502	8.0	4.0	2.40
6	9.257E+02	1.1148E-05	580.161	8.0	4.0	2.40
7	1.099E+03	1.2788E-05	590.156	8.0	4.0	2.40
8	1.084E+03	1.1481E-05	618.6	8.0	4.0	2.40
9	8.641E+02	1.2610E-05	527.009	8.0	4.0	2.40
10	8.978E+02	1.3986E-05	510.099	8.0	4.0	2.40
Without CNTs						
Sample	G_{IIC} (N/m)	C (m/N)	P_c (N)	L (cm)	a (cm)	b (cm)
1	6.181E+02	1.2315E-05	451.026	8.0	4.0	2.40
2	6.142E+02	1.2121E-05	453.201	8.0	4.0	2.40
3	7.960E+02	1.2392E-05	510.283	8.0	4.0	2.40
4	5.929E+02	1.0091E-05	450.409	7.5	4.0	2.40
5	6.796E+02	1.0395E-05	475.106	7.5	4.0	2.40
6	6.245E+02	1.0604E-05	450.901	7.5	4.0	2.40
7	4.611E+02	9.4162E-06	378.589	7.0	4.0	2.40
8	6.594E+02	9.4877E-06	451.02	7.0	4.0	2.40
9	6.475E+02	8.6505E-06	430.048	6.5	4.0	2.40
10	6.594E+02	9.2081E-06	420.631	6.5	4.0	2.40

F. PHASE V RESISTANCE TESTING FOR FIBERGLASS COMPOSITES WITH CNT REINFORCEMENT

Each coupon was tested three times (generally) using the following procedure:

1) Measure the crack length and initial resistance reading.

2) Load and unload the coupon allowing no crack to propagate.

3) Measure the resulting resistance reading.

Each of the rows below represents the different trial runs for each sample.

New Crack Length (cm)	Initial Resistance Reading (Ohms)	Load (N)	Final Resistance Reading (Ohms)	Percentage Change
Coupon 1 (Avg = 0.30%)				
6.4	44300	100	44500	0.45%
6.4	44500	100	44600	0.22%
6.4	44600	100	44700	0.22%
Coupon 2 (Avg = 3.49%)				
6.2	771100	100	820100	6.35%
6.2	739000	100	739200	0.03%
6.2	739200	100	709000	4.09%
Coupon 4 (Nonconductive after loading)				
6.5	285500	100	over 1 MΩ	N/A
Coupon 7 (Avg = 2.24%)				
6	912600	100	891200	2.34%
6	914400	100	908200	0.68%
6	904600	100	871100	3.70%

G. PHASE V RESISTANCE TESTING FOR CARBON FIBER COMPOSITES WITH CNT REINFORCEMENT

Each coupon was tested three times (generally) using the following procedure:

1) Measure the crack length and initial resistance reading.

2) Load and unload the coupon allowing no crack to propagate.

3) Measure the resulting resistance reading.

Each of the rows below represents the different trial runs for each sample.

New Crack Length (cm)	Initial Resistance Reading (Ohms)	Load (N)	Final Resistance Reading (Ohms)	Percentage Change
Coupon 1 (Avg = 0.29%)				
5.7	182.1	50	182.3	0.11%
5.7	180.8	50	181.8	0.55%
5.7	181.5	50	181.9	0.22%
Coupon 2 (Avg = 0.35%)				
5.5	28.9	50	28.8	0.35%
5.5	28.8	50	28.7	0.35%
5.5	28.8	50	28.9	0.35%
Coupon 3 (Avg = 1.08%)				
6.3	51.3	50	51.7	0.78%
6.3	50.5	50	51.6	2.18%
6.3	51.2	50	51.6	0.78%
6.3	51.2	50	51.5	0.59%
Coupon 4 (Avg = 0.20%)				
5.8	67.2	50	67	0.30%
5.8	67	50	66.9	0.15%
5.8	67	50	67.1	0.15%
Coupon 5 (Avg = 0.67%)				
5.6	365.1	50	370.1	1.37%
5.6	372.2	50	371.1	0.30%
5.6	370.1	50	371.4	0.35%

(Table G continued)

New Crack Length (cm)	Initial Resistance Reading (Ohms)	Load (N)	Final Resistance Reading (Ohms)	Percentage Change
Coupon 6 (Avg = 4.62%)				
6.1	93.5	50	101.7	8.77%
6.1	108.4	50	108.6	0.18%
6.1	99.4	50	103.2	3.82%
Coupon 8 (Avg = 0.33%)				
7.2	839.2	50	836.7	0.30%
7.2	840.1	50	846	0.70%
7.2	847.7	50	847.7	0.00%
Coupon 9 (Avg = 1.55%)				
6.6	157.7	50	163	3.36%
6.6	161.2	50	159.1	1.30%
6.6	160.5	50	160.5	0.00%
Coupon 10 (Avg = 2.66%)				
6.6	276.5	50	278.1	0.58%
6.6	276.1	50	276.6	0.18%
6.6	276.6	50	256.6	7.23%

APPENDIX B. ONE-SLIDE PROJECT SUMMARY

Damage Detection in Composite Interfaces through Carbon Nanotube Reinforcement

Young Kwon, Randall Pollak --- Funding Document #F1ATA09134G002

Damage Detection in Composite Interfaces through Carbon Nanotube Reinforcement

STATUS QUO

Modular Construction and Repair of Large Composite Sections

• Discontinuities in reinforcing fibers and stress concentrations are concerns at joints • Lack of confidence in structural integrity

Nanocomposites

• Nanoparticles improve interface strength • Dispersing nanoparticles throughout matrix is very costly, overdesigns large structures

Evaluation / Health Monitoring

• Traditional NDE methods challenging for heterogeneous materials at complex joints • In situ sensors generally reduce strength

NEW INSIGHTS

Carbon Nanotubes (CNTs)

• Significant improvement in fracture strength may be realized using CNT network along interface • Mechanical properties dependent on maintaining network • High electrical conductivity of CNTs can be exploited to monitor interfacial damage

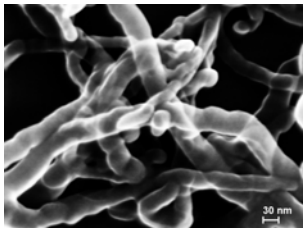

Scanning electron microscope image of dispersed CNTs

MAIN ACHIEVEMENTS:

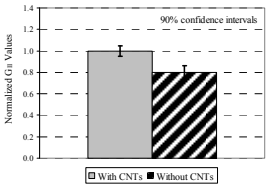

Application of CNTs along carbon fiber composite interface significantly improved Mode II fracture toughness

• Carbon and glass fiber composites fabricated using vacuum-assisted resin transfer molding • Demonstrated no weakening using two-step curing compared to co-cured samples • Application of dispersed CNT layer with two-step curing improved interfacial fracture toughness for both carbon and glass fiber composites • Electrical resistance shown to increase linearly with interfacial crack length for carbon fiber composite samples

CNTs dispersed on carbon fiber composite interface improved fracture strength while acting as *in situ* sensor

LIMITATIONS OF INITIAL STUDY:

• Focus on Mode II fracture under 3-point bend test • Used woven fabric composites with vinyl ester resin • Choice of CNT type and concentration based on fracture strength, not optimized for damage detection sensitivity

QUANTITATIVE IMPACT

Current Impact

• 25% improvement in Mode II critical strain energy release rate (G_{II}) for carbon fiber composite specimens using dispersed CNT layer • 54% improvement in G_{II} for glass fiber composite specimens when CNTs added • Interfacial damage across CNT layer can be monitored using electrical resistance (linear relationship demonstrated for carbon fibers with vinyl ester resin) • Baseline resistance and slope varies from sample to sample due to unique CNT dispersion for each sample

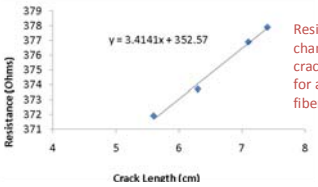

Resistance changes as crack grows for a carbon fiber sample

END-OF-PHASE GOAL

Planned Impact

• Initial feasibility study is completed showing application of CNTs can improve mechanical properties at critical interfaces while simultaneously providing means of monitoring damage at such critical interfaces

Future Research Goals

• Experimental investigation of relevant interfaces (e.g., adhesive joints, skin/core sandwich composites, etc.) • Multiphysics modeling of interfaces with nanoparticles • Prognosis capability for military applications

Publications and presentations from this project:

(1) Bily MA, Kwon YW, Pollak RD. "Study of composite interface fracture and crack growth monitoring using carbon nanotubes," *Applied Composite Materials* (accepted for publication, doi 10.1007/s10443-009-9124-4).

(2) Kwon YW, Bily MA, Pollak RD. "Preventing and monitoring crack growth in composite interfaces using carbon nanotubes," abstract submitted for 2010 National Space & Missile Materials Symposium.

THIS PAGE INTENTIONALLY LEFT BLANK

REFERENCES (ALPHABETICAL LISTING)

Ahmed, K., W. Pan, and S. Shi. 2006. Electrical Conductivity and Dielectric Properties of Multiwalled Carbon Nanotube and Alumina Composites. *Applied Physics Letters* 89.

Bily M.A., Y.W. Kwon, and R.D. Pollak. Study of Composite Interface Fracture and Crack Growth Monitoring using Carbon Nanotubes, *Applied Composite Materials* (accepted for publication, doi 10.1007/s10443-009-9124-4).

Burkholder G. L. "The Effects of Carbon Nanotube Reinforcement on Adhesive Joints for Naval Applications," Master's thesis, Naval Postgraduate School, 2009.

Callister, William D., Jr. *Materials Science and Engineering: An Introduction*, 7th ed., New York: John Wiley and Sons, Inc, 2007.

Chou, Tsu-Wei and Erik T. Thostenson. Carbon Nanotube/Vinyl Ester Nanocomposites for in Situ Sensing. September 17–19, 2008. University of Maryland University College, Adelphia, MD. *Office of Naval Research Solid Mechanics Program Review Meeting: Marine Composites and Sandwich Structures*.

Deng, F., and Q. Zheng. 2008. An Analytical Model of Effective Electrical Conductivity of Carbon Nanotube Composites. *Applied Physics Letters* 92.

Dharap, P., Z. Li, S. Nagarajaiah, and E.V. Barrera. 2004. Nanotube Film Based on Single-wall Carbon Nanotubes for Strain Sensing. *Nanotechnology* 15.

Faulkner, Susan. "Study of Composite Joint Strength with Carbon Nanotube Reinforcement," Master's thesis, Naval Postgraduate School, 2008.

Gates, Dominic. "Boeing 787 May not Fly this year," *The Seattle Times*, 22 Jul 2009.

Gounder, Raj. Senior Manager for Strategic Development, The Boeing Company. Personal communications at Boeng Tech Expo, 8 Aug 2008.

Government Accountability Office (GAO). NASA: Constellation Program Cost and Schedule Will Remain Uncertain Until a Sound Business Case Is Established. GAO Report 09-844, 25 Sep 2009.

Harris, P.J.F. 2004. Carbon Nanotube Composites. *International Materials Review* 49.

Jones, R., and H. Alesi. 2000. On the Analysis of Composite Structures with Material and Geometric Non-linearities. *Composite Structures* 50.

Jones, R., H. Alesi, W.K. Chiu, and S. Galea. 1995. A Preliminary Study into the Matrix Dominated Non-linear Behavior of Graphite/Epoxy Laminates. *Composite Structures* 30.

Kang, I., M.J. Schulz, J.H. Kim, V. Shanov, and D. Shi. 2006. A Carbon Nanotube Strain Sensor for Structural Health Monitoring. *Smart Materials and Structures* 15.

Kwon, Y.W., R. Slaff, S. Bartlett, and T. Greene. 2008. Enhancement of Composite Scarf Joint Interface Strength through Carbon Nanotube Reinforcement. *Journal of Materials Science*.

Lu, C., and Y. Mai. 2008. Anomalous Electrical Conductivity and Percolation in Carbon Nanotube Composites. *Journal of Materials Science* 43.

Messinger, R. Evaluation of Advanced Composite Structures Technologies for Application to NASA's Vision for Space Exploration. NASA Technical Report, NASA/CR-2008-215120, Jul 2008.

Mouritz, A.P., E. Gellert, P. Burchill, and K. Challis. July 2001. Review of Advanced Composite Structures for Naval Ships and Submarines. *Composite Structures* 53.

Nofar, M., S.V. Hoa, and M.D. Pugh. 2009. Failure Detection and Monitoring in Polymer Matrix Composites Subjected to Static and Dynamic Loads Using Carbon Nanotube Networks. *Composites Science and Technology*.

Saito, R. and M. S. Dresselhaus. Physical Properties of Carbon Nanotubes. 1998. Imperial College Press.

The Venton Research Group. Development of Carbon Nanotube Modified Microelectrodes. n.d. http://www.faculty.virginia.edu/ventongroup/nanotube.html (accessed September 9, 2009).

Thostenson, E.T., and T.W. Chou. 2006. Carbon Nanotube Networks: Sensing of Distributed Strain and Damage for Life Prediction and Self Healing. *Advanced Materials* 18.

Thostenson, E.T., and T.W. Chou. 2008. Carbon Nanotube-based Health Monitoring of Mechanically Fastened Composite Joints. *Composites Science and Technology* 68.

Todo, M., T. Nakamura, and K. Takahashi. 2000. Effects of Moisture Absorption on the Dynamic Interlaminar Fracture Toughness of Carbon/Epoxy Composites. *Journal of Composite Materials* 34.

Weber, I., and P. Schwartz. 2001. Monitoring Bending Fatigue In Carbon-Fibre/Epoxy Composite Strands: A Comparison Between Mechanical and Resistance Techniques. *Composites Science and Technology* 61.

Wong, M., M. Paramsothy, X.J. Xu, Y. Ren, S. Li, and K. Liao. December 2003. Physical Interactions at Carbon Nanotube-Polymer Interface. *Polymer* 44.

Zhang, W., V. Sakalkar, and N. Koratkar. 2007. In Situ Health Monitoring and Repair In Composites Using Carbon Nanotube Additives. *Applied Physiscs Letters* 91.

INITIAL DISTRIBUTION LIST

1. Defense Technical Information Center
   Ft. Belvoir, Virginia

2. Dudley Knox Library
   Naval Postgraduate School
   Monterey, California

3. Research Office, Code 41
   Naval Postgraduate School
   Monterey, California

4. Dr. David Stargel
   Air Force Office of Scientific Research
   Arlington, Virginia

5. Professor Young W. Kwon
   Naval Postgraduate School
   Monterey, California

6. Lt Col Randall D. Pollak
   Naval Postgraduate School
   Monterey, California

7. Professor and Chairman Knox T. Millsaps
   Naval Postgraduate School
   Monterey, California

THIS PAGE INTENTIONALLY LEFT BLANK